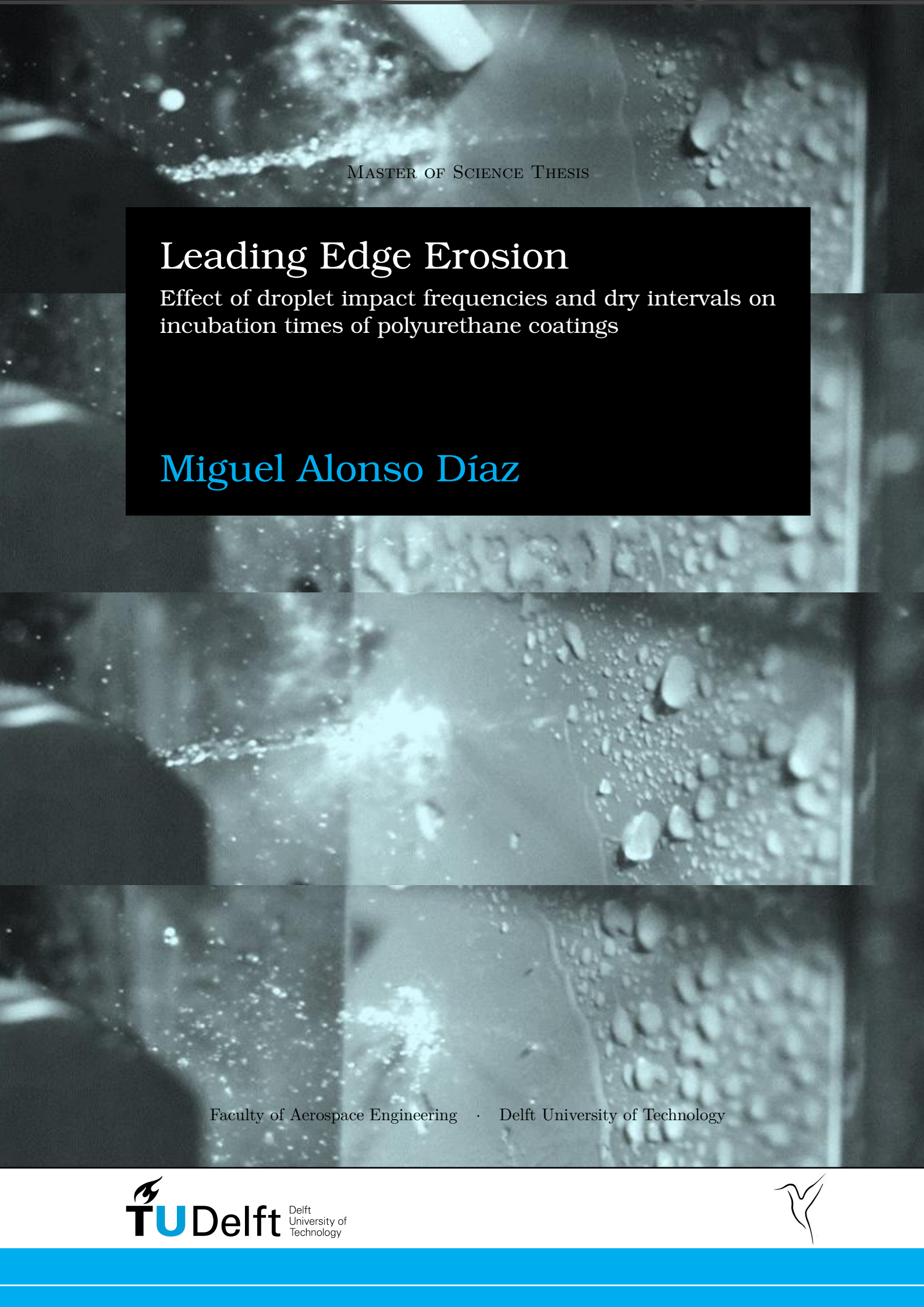

Master of Science Thesis

Leading Edge Erosion

Effect of droplet impact frequencies and dry intervals on incubation times of polyurethane coatings

Miguel Alonso Díaz

Faculty of Aerospace Engineering · Delft University of Technology

TU Delft Delft University of Technology

Leading Edge Erosion

Effect of droplet impact frequencies and dry intervals on incubation times of polyurethane coatings

Master of Science Thesis

For obtaining the degree of Master of Science in Aerospace Engineering
at Delft University of Technology

Miguel Alonso Díaz

August 2021

Faculty of Aerospace Engineering · Delft University of Technology

Delft University of Technology
Faculty of Aerospace Engineering
Department of Aerospace Structures and Materials

GRADUATION COMMITTEE

Dated: August 2021

Chair holder:

Dr.ir. R.C. Alderliesten

Committee members:

Dr. J.J.E. Teuwen [Daily Sup.]

Dr.ir. J.A. (John-Alan) Pascoe

Dr. A. (Amrit) Verma [Daily Sup.]

Abstract

Rain erosion of leading edges in wind turbines caused by high-velocity droplet impacts is one of the current problems in wind energy that affects their energy production and maintenance costs. The most widespread solution for this problem is the application of viscoelastic coatings (generally, polyurethane) along the leading edge of the wind blade, the area that first meets the raindrop.

The focus of the present study is to assess experimentally the effect of the frequency of droplet impacts and the performance of dry intervals (this is, intervals of time at which the test stops) on the incubation times of industrial viscoelastic polyurethane PU coatings. The coated samples were tested in a Pulsating Jet Erosion Tester (PJET) facility. The incubation times, defined as the period of time until damage is observed in the material, were measured in number of impacts and in global testing time (time that the test was kept running) until damage. The two effects that are aimed to investigate, the droplet impact frequency and the dry intervals, represent different relaxation times that the coating may undergo under real-life rainfall conditions: time intervals between individual raindrops (between raindrops) and between rain events (between rainfalls). Higher relaxation times are expected to have a beneficial effect on the rain erosion performance, as the viscoelastic coating would have time to recover itself to the original stress and strain state. The effects of test conditions that may influence the PJET, such as the water cushion effect, temperature and humidity were considered and evaluated.

It was found that droplet impact frequency has an effect on the number of impacts until incubation: the lower the impact frequency, the lower the number of impacts until incubation. This effect has been linked to the longer and more energetic droplets produced by the PJET for these low frequencies and is not related to the viscoelastic behaviour of the coating. The existence of dry intervals when testing significantly increased the incubation times of PU coatings. This increase was larger when the dry intervals had a longer duration and when they were performed earlier during the tests. The effects of dry intervals in incubation times have been linked to the viscoelastic behaviour of the polyurethane coating. These results are expected to shed light on the effects of testing variables (impact frequency and dry intervals) that have historically been ignored in rain erosion tests and will help the design of new test parameters for erosion testing. The conclusions of the work will help to understand the importance of relaxation times and viscoelasticity in the incubation time of PU coatings and reveal that these effects will help to refine models that aim to predict the lifetime of polyurethane coatings in wind blade turbines based on real-life rainfall data.

While investigating the influence of impact frequency, effects that may affect the PJET results were investigated. The effect of the water cushion was evaluated. This phenomenon consists of a water film that remains on the coating and that affects the posterior droplet impact. Water cushion effects were found to slightly increase incubation times for the highest impact frequencies. Their effects were counteracted with an air supplier aimed at the tested sample which removed the water cushion. Humidity and temperature were found to have an effect on the incubation times: in general, the higher the temperature and the relative humidity, the shorter the incubation times. The incubation times of saturated samples which went through humidity treatments were tested: their incubation times were lower than for those samples which did not undergo that treatment. DMA analysis was performed on PU samples, but the change in mechanical properties of the coating could not be directly linked to the drop in incubation times. It is suspected that plasticization is affecting the mechanical properties of the coating. The change in the environmental conditions may also be affecting the adhesion between the coating and substrate, resulting in lower incubation times.

Table of Contents

List of Figures

List of Tables

Nomenclature

Symbol	Meaning
a	Eisenberg's $D - v_i$ linear constant
C_C	Velocity of sound in the coating
C_L	Velocity of sound in the liquid
C_S	Velocity of sound in the substrate
D	Erosive damage
d_d	Droplet diameter
d	Hole diameter (rotating disk geometry)
E'	Storage modulus
E''	Loss modulus
f_{disc}	Rotational frequency of the PJET disc
f_i	Droplet impact frequency
h_c	Thickness of the coating
h_s	Thickness of the substrate
k	Constant in Power law for Wöhler; constant value for power law equation
l_d	Droplet length
m	Wöhler's slope of the material
n	Eisenberg's $D - v_i$ power law constant (6.7)
n_f	End of the steady erosion rate period (Springer's model)
n_i	Number of impacts until damage (incubation)
n_i^*	Number of drops impinging per site until damage (incubation)
P	Impact pressure (homogeneous model)
r	Ratio between incubation times
r_{disc}	Distance from the centre of disk to hole (geometry)
S	Springer's strength parameter (homogeneous model)
S_e	Springer's strength parameter (coated model)
t_{dry}	Length of the dry interval
$t_{dry\,0}$	Moment at which the dry interval starts
t_i	Global testing time until incubation
$t_{i\,(ref)}$	Global testing time until incubation used as reference: without dry intervals
$t_{i\,(stops)}$	Global testing time until incubation in which dry intervals were performed
v_i	Droplet impact velocity
α	Dry interval parameter (see Equation 2.10)
β	Dry interval parameter (number of stops)
λ	Dry interval parameter (see Equation 2.9)
μ	Mean (parameter lognormal distribution)
ν	Poisson's ratio
ρ_c	Density of the coating
ρ_L	Density of the liquid
ρ_S	Density of the substrate
σ	Variance (parameter lognormal distribution)
σ_u	Ultimate tensile strength
σ_0	Mean stress at the liquid-coating interface (coated model)

Abbreviation	Meaning
CTS	Clima Temperatyre System
DMA	Dynamic Mechanical Analysis
GFRP	Glass Fibre Reinforced Plastic
MAD	Median Absolute Deviation
LEE	Leading Edge Erosion
PJET	Pulsating Jet Erosion Tester
PU	Polyurethane
TTS	Time-temperature superposition (principle)
WTB	Wind Turbine Blade

Acknowledgements

I would like to take this opportunity to sincerely thank my supervisors, Julie Teuwen and Amrit Verma for their assistance during my work on this thesis. The guidance, feedback and help that you have provided to me are invaluable. Thank you to the rest of the TU Delft team that has supported me during my work: to the AMT department, teachers and staff at the lab.

Thank you very much to every people that had supported me to during all this time. Thank you very much to my mom, for her love and unconditional encouragement in every step that I have made. To Alba, thank you for your support all this time. And many thanks to Huub and all my good friends that have come with me on the journey.

Delft, University of Technology
August 2021

Miguel Alonso Díaz

Chapter 1

Introduction

1.1 Background

Wind energy use has experienced a sharp rise in the latest years, with approximately an increase of 10% of global wind turbines installation every year [11]. This increase is in large part a result of political, social and economic pressure to find renewable and alternate energy resources, as well as an important development in the material industry that has driven wind energy to be more economically viable. Current trends are directed to make larger wind turbines with larger rotor diameters to raise their efficiency, which usually comes along with a higher wind blade tip velocity [3]. Figure 1.1 shows the evolution in size and energy output for wind turbines for the last years. The tip velocity of current wind blades can range between 70 and 110 m/s. Figure 1.2 shows the maximum wing-tip speed against wind turbine rotor diameter for various manufacturers.

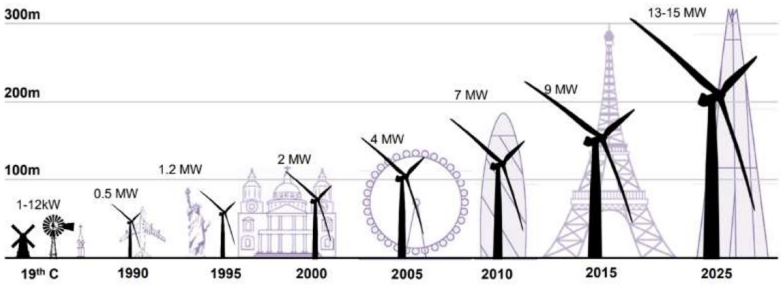

Figure 1.1: Evolution of the wind turbine in MW output and size. Source: [1]

A higher wind-tip velocity means that, in presence of rain, the impact velocity of a raindrop will be higher. Another current trend is to build offshore wind turbines, as they are in general subjected to steadier wind, producing more and more stable power while offering other benefits such as a not so strict noise regulation [12]. However, offshore locations are considered to potentially have a more hostile environment regarding rain erosion than onshore

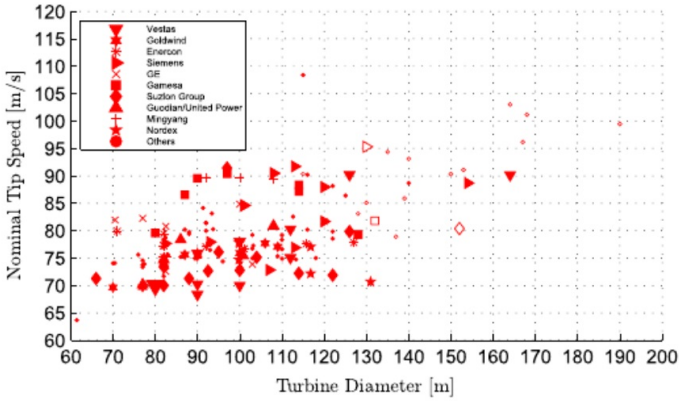

Figure 1.2: Maximum wind blade tip velocity on rotor diameter for wind turbines with greater capacity than 1 MW. Source: [2]

located wind farms [3]. These trends: larger wind blades that lead to a higher speed, increase in offshore wind farm locations and even the wind energy market expansion to other world regions in which rainfall is more common, such as Asian markets, have caused rain erosion to be a current problem for wind turbines. The leading edge of a wind turbine is the area that first meets air and also the first to show damage, the problem is often called Leading Edge Erosion (LEE). The effects of this phenomenon can be seen in Figure 1.3.

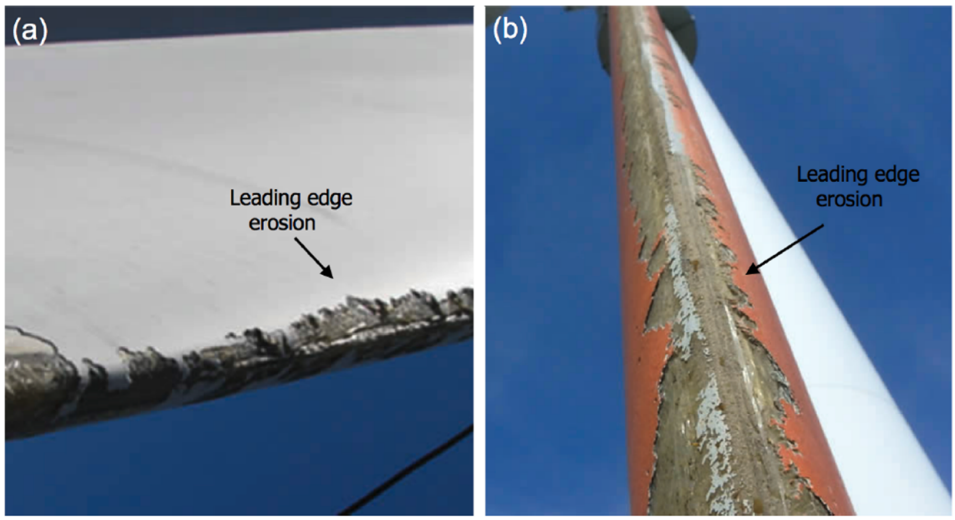

Figure 1.3: Leading Edge Erosion effects. Source: [3]

LEE affects the overall wind blade performance. The roughness and imperfections induced by rain erosion result in a larger drag force and lower lift. Experimental research on a typical wind blade profile has shown that LEE may lead to a 6-500% drag increase of the blade, depending on rain intensity, ranging from light to heavy rain [13]. Computational Fluid Dynamics numerical simulations performed on typical wind turbine profiles suggest that the drag coefficient may be increased up to 314% and the lift coefficient reduced by 53% in presence of rain erosion for the whole blade [14]. It has been estimated that LEE could cause

a loss in energy production of about 25% due to these effects [13]. Furthermore, rain erosion has repercussions on the maintenance costs [15], enhanced by the fact that wind turbines maintenance is usually difficult to carry on. Wind turbines farms tend to be in not very accessible locations (especially in offshore locations), the repair materials may need to meet some environmental requirements for their correct application. All these factors are challenges for the reparation of wind turbines.

The LEE phenomenon involves different phenomena. When a high-velocity water droplet impacts against a coating, a pressure (the so-called water-hammer pressure) appears on its surface [16]. After the impact, different shock waves are created and travel through the coating: compressive, tensile and Rayleigh stress waves which may cause initial imperfections in the surface [4]. The droplet is also subjected to compressive stress. A high-pressure compressive wave travels through the droplet. The evolution of this compressive area is shown in Figure 1.4. Once the stress wave reaches beyond the point where the droplet meets impacting surface (represented in the Figure 1.4 b), the pressure is released and water is expelled sideways at very high velocities [17]. This process is known as lateral jetting. Lateral jetting velocities may go up to six times the initial droplet velocity [18], with the pressures in this waterfront can be three times higher than the initial water-hammer pressure [19]. Lateral jetting can strip away imperfections present in the surface caused by stress waves, increasing surface roughness and ultimately, leading to mass loss of the coating [20]. After a droplet impact, a thin film of water may get adhered to the coating just before the next impact. This water film has been found to damp next impact, lowering the water-hammer pressure [21] and reducing lateral jetting flow rate [22]. This is the so-called "water cushioning" effect and is not likely to happen in a real-life wind blade due to the wind blade rotating at high speed [23]. However, it could happen in some experimental erosion setups.

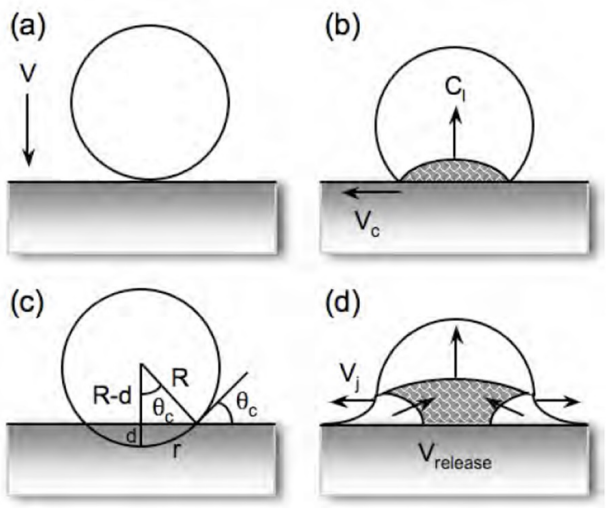

Figure 1.4: Lateral jetting generation after impact. The compressive stress region in the droplet is marked in grey. Source: [4].

One of the most widespread solutions to avoid and delay LEE is the application of Leading Edge Protection (LEP) systems in the form of coatings or shields on the wind blade leading edge. Gelcoats are used to protect the whole blade, while the coating located at the Leading

Edge consists of more flexible materials, mainly polyurethane (PU) coatings. Gelcoats consist of a similar material to the structure matrix material, usually, epoxy or polyester [24]. These coatings are usually applied with an in-mould technique, at the same time that the rest of the wind blade structure. Gelcoats have high stiffness and offer high adhesion to the composite blade substrate. On the other hand, PU coatings are more flexible, viscoelastic, and are applied after the manufacture of the wind blade, post-mould. Multilayered systems are usually applied to improve their adhesion to their substrate [3]. Figure 1.5 shows different methods to apply these wind blade coatings.

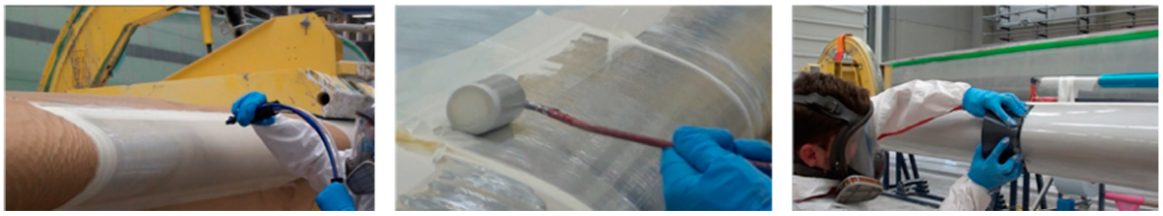

Figure 1.5: Three post-mold application techniques for flexible polyurethane coatings: spray (a), roller (b), and trowel (c). Source: [5].

Rain is a stochastic process and it is defined by statistical distributions [25]. Many rainfall parameters, such as rainfall intensity, impact frequency and droplet diameter, are random. During a rain event, there are changes in intensities and "dry intervals" may appear in which rain stops for a while [26]. These changes in rainfall intensity and in rainfall duration can be observed in Figure 1.6, which shows a real-life rainfall record in the airport of Schiphol during 12 hours. As rainfall is stochastic, wind blade coatings are subjected to a range of impact frequencies caused by raindrops. This would mean variable relaxation times between raindrop impacts. It has been theorized that viscoelastic coatings need to have a relaxation time after an impact to recover themselves before the next droplet hit, improving their rain erosion performance. The effect of the dry intervals mentioned above may also affect the rain erosion performance of the coating: these dry intervals may cause the viscoelastic material to recover itself [27] and last longer. The effect of such changes of rain intensity is expected to depend on the material properties [28].

Erosion is an accumulative process. Several stages can be categorized during the rain erosion process, each of them with a different erosion rate. Authors, such as Heymann [19] divide the curve into five main stages; incubation, acceleration, maximum erosion rate, deceleration, and terminal erosion. Typically, the erosion process begins with barely visual damage on the surface: roughness is expected to increase, but the mass loss is not measurable. This stage is known as the incubation period. Quite a few researchers suggest that the incubation period is one of the best parameters to characterize rain erosion performance [29] and critical for wind turbine applications [23]. However, for some experimental tests, the incubation period may be short or even non-existent [7]. After the incubation period, the surface material starts to yield, roughness is increased due to the continuous droplet impacts and lateral jetting strips out imperfections, forming pits and leading to mass loss [17]. The pits eventually coalesce and form a crater. Mass loss keeps increasing until a steady mass loss rate is achieved. The mass loss rate finally declines after the crater has achieved a certain depth. Figure 1.7 represents a schematic evolution of cumulative erosion over time.

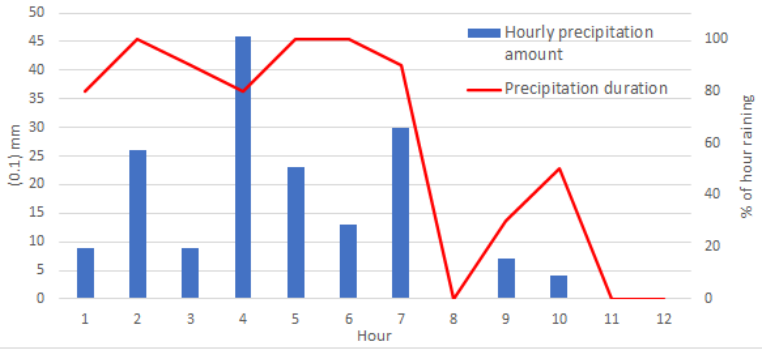

Figure 1.6: Rainfall data from the Schiphol airport (Netherlands) during 12 hours (recorded on 22/5/2021). The hourly precipitation amount and the precipitation duration during the hourly division are presented. Source: [6]

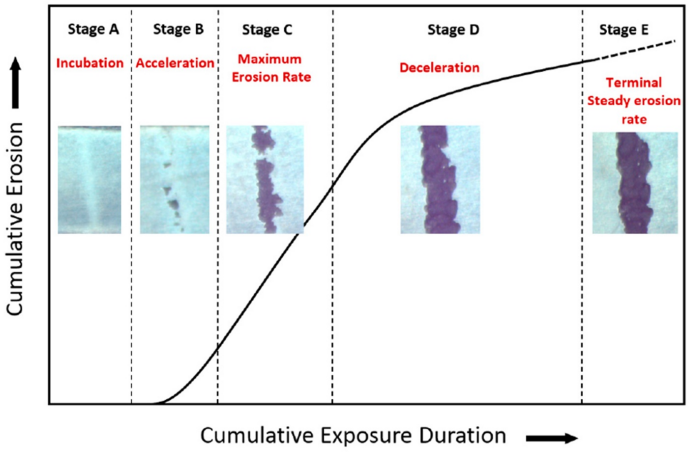

Figure 1.7: Accumulative erosion versus time. The representative stages of the erosion process are observed. The graph was built with experimental data from titanium samples tested at 300 m/s. Figure from [7]

Fatigue mechanisms have been historically considered analogous to erosion damage processes, mainly due to the repetitive nature of both phenomena: a repetitive load that leads to failure and damage after many cycles. This similarity has made researchers suggest a curve similar to the characteristic $S-N$ curve in fatigue which displays cyclic stress loading (S) against the number of cycles necessary for crack initiation (N) [30]. This curve, also called the Wöhler curve, can be adapted to the rain erosion problem. The result is a curve that links the number of droplets until damage initiation in coating with the droplet impact velocity: the $v_i - n_i$ curve [31]. The slope of the $v_i - n_i$ curve has been proven to be a very important parameter to understand the rain erosion behaviour of materials [25]. Other factors link rain erosion to fatigue, such as the existence of a threshold droplet impact velocity below which no erosive damage is observed. This feature is similar to the fatigue limit threshold. Fatigue has been inclined to be one of the driving mechanisms in rain erosion, but other phenomena, such as lateral jetting are just as important [7].

Erosion prediction models were developed based on fatigue, such as Springer's model [32].

This model was proven to correlate a large amount of erosion data and was developed for homogeneous materials, composites, and coated materials [7]. Springer's model considers that the damage evolution of the material (mass loss m) can be approximated as two straight lines as shown in Figure 1.8. Then, the erosion evolution is characterized by the incubation time (n_i in the Figure), the erosion rate (α) and the moment at which erosion starts decelerating (n_f). The analysis carried out by Springer et al. is based on the linear accumulative fatigue damage, the Palmgren–Miner rule, characteristic of fatigue damage [33]. Springer's model has been proved to model accurately damage progression when applied to polymer coatings used in the wind industry: Eisenberg et al. [30] applied Springer model to more than 200 wind turbines, finding a high correlation. Springer's model has also been validated when investigating rain erosion testing at laboratory PJET facilities [25]. Other models based on accumulative fatigue damage have been developed, for example, by Slot [29], which mainly considers the contribution to the stress by Rayleigh's stress waves.

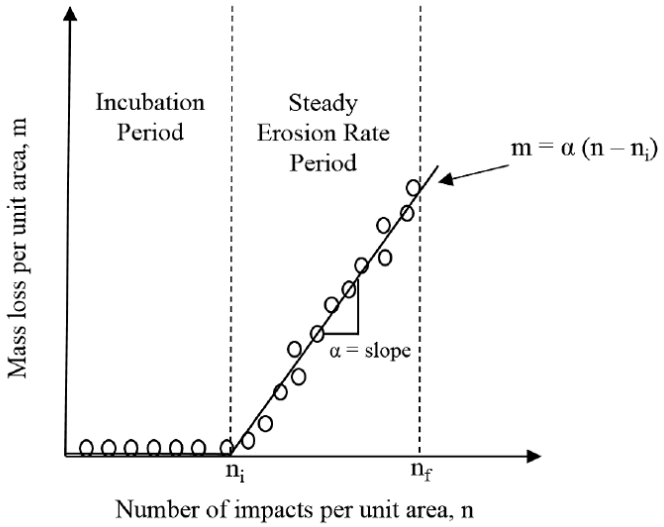

Figure 1.8: Schematic of Springer's solution model. Source: [7]

Springer's model is able to predict the incubation time and the erosion rate when given different material and testing parameters. Springer's prediction for the number of impacts until incubation time (n_i^*) for a homogeneous material is given by the following equation [34].

$$n_i^* = 7.1 \cdot 10^{-6} \cdot \left(\frac{S}{P}\right)^{5.7} \tag{1.1}$$

Where S is the strength parameter defined by Springer that depends on the material and P is the impact water-hammer pressure.

$$S = \frac{4\sigma_u(m-1)}{1-2\nu} \tag{1.2}$$

$$P = \frac{\rho_L C_L v_i}{1 + \frac{\rho_L C_L}{\rho_C C_C}} \tag{1.3}$$

The parameters S and P depend on the impact velocity (v_i) and different properties of the liquid (water) and the material: the velocity of sound in the liquid and the material (C_L, C_C), their density (ρ_L, ρ_S), the ultimate tensile strength of the material (σ_u), its Poisson's ratio (ν) and the Wöhler's curve slope for the tested material (m). Given these parameters, the model is expected to predict the number of impacts until incubation for a homogeneous material.

For a coated material, the equations are changed to account for the different impedances of the coating material and substrate and to consider the stress waves reflections in their interphase. These changes introduce modifications in the strength and impact pressure parameters, now called S_e (Springer's strength parameter) and σ_0 (mean stress at the liquid-coating interface). The complete form of the expressions for S_e and σ_0 can be found in [35].

$$n_i^* = 7.1 \cdot 10^{-6} \cdot \left(\frac{S_e}{\sigma_0}\right)^{5.7} \tag{1.4}$$

During the last decades, different experimental set-ups have been developed to investigate rain erosion. The underlying principle is the same in all of them: liquid is propelled into a sample, or the sample is moved towards the liquid [17]. Two different facilities stand out as prominent to study rain erosion: the water jet and the whirling arm. The water jet equipment consists of a nozzle that accelerates water towards the target surface. The whirling arm is based on a rotating arm that moves a sample under a waterfall. Researchers suggest that those two facilities cannot be correlated, at least directly [9], as droplet impact mechanisms, the nature of the damaged area and the profile of the damages are very different [36] [23]. It has been argued that more standardization may be necessary when regarding rain erosion facilities. Bartolomé et al. [37] proposed that the traditional approach to characterize erosion evolution (mass loss versus test time, or average erosion depth versus time) may ignore other important parameters, such as the impacting water volume or droplet impact frequency. The number of impacted droplets may be a better independent variable to represent mass loss. One of the main challenges of rain erosion research is the lack of correlation studies between different experimental types of equipment and with real-life conditions [37] which may prevent industry to get useful information from accelerated rain erosion tests. Recent efforts in standardization may help in this regard, but further actions are needed by many actors (companies, universities, and standardization committees) to have a better understanding of the phenomenon [29]. With all their drawbacks, rain erosion experiments still remain crucial to compare different materials and to provide data to models that aim to predict erosion life.

Springer's model equation already suggests that droplet impact velocity affects the incubation time of materials subjected to rain erosion. This is one of the more significant parameters in rain erosion [19]. Eisenberg et al. [30] analytically deduced that erosive damage has a power law with velocity, with the form:

$$D = a v_i^n \tag{1.5}$$

being D erosive damage, v_i impact velocity and a and n constants depending on the surface material. Eisenberg reported a value of $n = 6.7$ for LEE applications.

More parameters can affect the related damage mechanisms of rain erosion, such as droplet size: a larger droplet is expected to create erosion damage faster [38]. The droplet impact

angle has also been found to have an influence, being the stresses and damages maximum for impacts normal (90°) to the surface [38].

Rain erosion may also be influenced by droplet impact frequency [23]. This may be true especially for viscoelastic materials, such as flexible PU coatings. According to Engel et al. [27], viscoelastic properties of these coatings would imply that there is time for the material recovery from one impact to the next one: the material would have time to dampen the energy in that time and recover for the next impact. However, if impact frequency is too high, recovery may not be possible and strains may build up leading to damage. This strain build-up is shown in Figure 1.9. Real-life droplet impact frequency is very difficult to obtain in rain erosion experimental facilities. Rain erosion testing approaches rely on an accelerated rain erosion test approach: the induced droplets have a much higher impact frequency and velocity than in real life to speed up the tests and make them feasible. While it has been estimated that real-life raindrops impact frequency ranges between 0.05 and 5 Hz depending on the rainfall conditions [8], impact frequencies in a testing facility are higher: in the case of the PJET used in the present project, the frequency could be set between 2.3 and 47.4 Hz. In real life, viscoelastic materials have more time to recover between droplet impacts than in experimental setups. Similarly, impact velocities are much higher for accelerated testing: wind blades tip velocity can be up to 110 m/s, while most rain erosion facilities operate at 150-170 m/s [7]. These differences make it difficult to establish direct comparisons between rain erosion tests facilities and real operation rain erosion performance.

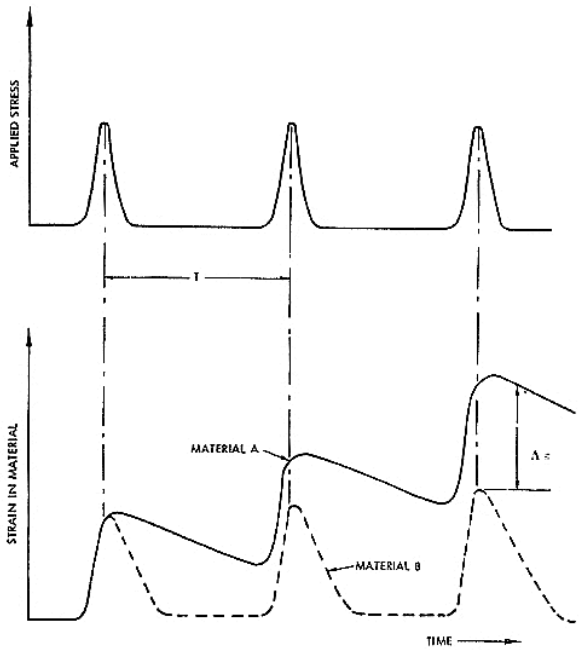

Figure 1.9: Effect of viscoelasticity and the evolution of the strains in a coating material. Strain evolution of two different viscoelastic materials with different relaxation times are presented: τ_A and τ_B. If the relaxation time of the material is larger than the time T, strain buildup will occur (material A). If it is shorter, material strains will be more limited (material B). Figure from: [8]

Raindrops impact frequency is theorized to have an important effect on viscoelastic PU coatings in wind turbines [27], as more time is given to the material to recover itself from the

last impact. However, this influence has not been yet the main focus of any research project. Furthermore, impact frequency has not been given enough attention when experimenting: standards for rain erosion testing still lack information about impact frequency [37]. The present current work will study experimentally how impact frequencies affect the incubation times of PU coatings. For this regard, a Pulsating Water Erosion Tester (PJET) facility installed at the faculty of TU Delft will be used. The effect of the performance of dry intervals while testing will also be studied: these intervals are also expected to help the coating similarly recover itself. These two features, the impact frequency and the existence of dry intervals can give a general glimpse of the different relaxation times that a coating undergoes under real-life rainfall conditions.

1.2 Research Objectives

The main research objective of the present research work is:

> "To investigate how rain droplet impact frequencies and the presence of "dry intervals" affect the incubation times in WTB's polyurethane coated samples by experimental procedures, using an accelerated jet erosion facility."

A study of the influence of impact frequency on the incubation times is expected to shed light on the behaviour of viscoelastic materials and will provide useful information for the design of rain erosion experiments. This study will help in the selection of parameters that have to be considered while testing in PJET facilities and will help in the standardization of testing procedures. Although the viscoelastic behaviour has been theorized to affect rain erosion [8] [27] and impact frequency has been varied in previous research studies when comparing different erosion tester types of equipment [23], to the best of the author's knowledge, the effect of impact frequency on incubation times has not been the focus of any research study.

Similarly, during real-life rainfall, some "dry intervals" between rainfalls and changes in intensity are expected to occur, since rainfall is a stochastic phenomenon [26]. These intervals may affect viscoelastic coatings in a similar way, as the coating would have more time to recover itself. Furthermore, they would represent the real operations of a wind blade much better. Three parameters have been used in the present work to characterize the dry intervals while testing: λ, α and β. The parameter λ accounts for the duration of the dry interval. The value α defines the moment at which the dry interval starts once the testing has started. Finally, β represents how many stops are performed, this is, the number in which the dry interval is divided. These parameters should give a general overview of the different kinds of dry intervals that could happen during real-life rain: those intervals could last longer, start sooner once rainfall has started or be more intermittent (see the change in rain intensity and moments where rain stops in Figure 1.6). No literature research has been found that addresses the influence of these dry intervals in the incubation time of viscoelastic coatings. These results will be useful when considering parameters and the logistics for rain erosion testing.

The results of this work will be useful for the design of experiments and standardization of testing procedures at PJET facilities, helping the definition of testing parameters that may affect testing results. They will also are expected to trigger more experimentation over the

influence of impact frequency and dry intervals on viscoelastic coatings. Further work on the subject will help to refine models aimed to predict the lifetime of wind blade coatings subjected to rain that uses stochastic real-life rainfall data and accounts for different impact frequencies and dry intervals. The findings will also help to interpret rain erosion models that do not account for dry intervals in viscoelastic coatings and that just consider the number of impacts (for example, Springer's model).

1.3 Research questions and hypotheses

The two main Research Questions for the current research project are formulated:

> "How do different droplet impact frequencies affect the incubation time of viscoelastic PU coatings?"

> "How does the existence of "dry periods" affect the incubation time of viscoelastic PU coatings?"

These two effects are both linked to the viscoelastic behaviour of the PU coating which is being tested. The results of these tests are expected to link rain erosion testing with real-life rainfall conditions. Only PU flexible coatings have been tested. Each question can be divided into different sub-questions. Related to the first Research Question that tackles the effect of impact frequencies:

> "How do incubation times of PU coatings vary when changing impact frequency? How does it change with velocity?"

> "How can this trend affect the results of semi-empirical models that are used to predict the lifetime of WBT coatings (Springer's model)?

A lower impact frequency is expected to improve the erosion performance of the PU coating and thus, raise the number of impacts until incubation time. This is expected due to the extra time that the coating will have to recover itself between impacts. Higher velocities imply larger impact pressures which cause larger stresses and strains. Larger stresses will mean that the coating needs more time to recover itself until the next impact. This effect for high velocities is expected to be observed especially when droplet impact frequency is high and there is not much time for the coating to recover, but it could be observed also for lower frequencies. Semi-empirical models such as Springer rely on experimental data: if frequency plays a role, higher frequency tests are expected to have a lower incubation time than predicted, and for lower frequency, higher times.

The sub-questions that are related to the second main Research Question, the one which addresses the existence of dry intervals while testing, are shown below:

> "How the different "dry interval" parameters that characterize the impact (λ, α, β) affect the incubation times of PU coatings?"

> "How can the results be linked to the viscoelastic behaviour of PU? Can they be linked to other phenomena?"

Longer dry intervals (this is, stops with a larger λ) are expected to rise the incubation times more since the coating will have more time to recover itself. The time at which the dry interval starts once the test has already started is expected to have. This feature is represented with the parameter α. Lower values of α will mean that the stop has been carried out early while testing and larger values of α will mean that the stop has been executed later. If the dry interval starts later, it could happen that the coating had already undergone enough droplet impacts to be plastically deformed. If this happens, the coating would be not expected to recover itself completely. On the contrary, if the dry interval starts earlier, plastic damage could have been avoided, and the coating may have recover itself. Then, lower values of α are expected to improve rain erosion performance and thus, rise incubation time. The number of parts in which the dry interval will be divided (for a given duration of the dry period) is given by β. This parameter could be significant if the incubation times are sensitive to the distribution of the dry interval in time. The results will be explained based on the viscoelastic nature of the material.

During the experiments, it was observed that the incubation times measured at the beginning of the day were considerably lower than the incubation times that were recorded at the end. The effects of temperature and humidity were investigated: how the mechanical properties of saturated PU coatings change compared to dry PU coatings and when the temperature is increased.

Chapter 2

Methodology

The methodology of the research study is addressed in the following chapter. First, the experimental setups that have been used are presented. Then, a review of the principal analytical methods considered during the thesis is presented. Finally, the test plan that was followed during the research work is presented.

2.1 Experimental

This section is focused on the experimental aspect of the thesis. First, the samples that were tested are presented. Then, the main equipment used to carry on the experiments is introduced: the PJET, the high speed camera, the thermocouples, microscope, the Clima Temperature System (CTS) and the Dynamic Mechanical Analysis (DMA) equipment.

2.1.1 Test samples

Polyurethane based coated samples were used. The substrate consisted of Glass Fibre Reinforced Plastic (GFRP) that was manufactured in-house facility using a vacuum infusion process. The layup sequence that was used is characteristic of real-life composites located at the leading edge of a wind turbine blade. The samples were shipped to the PU coating supplier to apply the industrial coating. The applied coating is W4600 WBPC, a two-component polyurethane coating. Its glass transition temperature (T_g) its $-5°$ according to its datasheet [39]. The characteristic thickness of the PU coating was about 0.3 mm in the tested samples (0.31 ± 0.04 mm), while the thickness of the substrate is about 2.5 mm (2.53 ± 0.03 mm). The recommended thickness of the coating present in the datasheet ranges from 0.25 to 0.35 mm [39]. Figure 2.1 shows a cross-section of one of the coated samples. Table 2.1 shows the properties of the PU coating that were needed to characterize the material and required for Springer's model. Some of them were obtained from the literature.

To process the results in Springer's model, the density and the speed of the sound of the GFRP substrate were needed. The density of the substrate was measured by performing measures

ρ_c	C_c	σ_U	μ
1100 kg/m^3 [3]	1900 m/s [40]	37 MPa [39]	0.3 [3]

Table 2.1: Properties of the polyurethane coating

of a sample of the substrate in air and distilled water at a known temperature. Springer [34] suggests a value for the velocity of sound in GFRP substrates: 2270 m/s. The speed of sound was also experimentally measured using ultrasonic testing: an Olympus (SNW1-0L-WP5) standard wedge probe was used, its frequency set at 2.25 MHz. The sound velocity of the substrate measured with this setup was 5000 m/s. This value is quite different from the velocity of 2270 m/s suggested by Springer. It was decided to select the average value between the two values and consider the deviation when using this value. For this reason, the results that use this value are affected by this high deviation. Properties of the substrate are shown in Table 2.2.

ρ_s	C_s
1840 kg/m^3 [3]	3600 m/s

Table 2.2: Properties of the GFRP substrate

The batches of GFRP coated with PU were cut with a square shape to be placed in the PJET, see Figure 2.1 (size of the samples: $[8.9 \pm 0.6]$ x $[8.4 \pm 0.4]$ mm). To reduce scatter due to the variability of the coating (accounting for defects that may be present just in some batches), samples of different batches were alternated when testing. A matrix modulation approach was used to test the PU samples: the square sample was divided into 16 different test points. Each of the points was tested in the PJET for different impact parameters and represented a single measured data point. The impact matrix approach is shown in Figure 2.1. The impact points were checked to be far enough from the sample edges to avoid any edge effect. They remained also far away from each other. Before testing, samples were visually inspected in search of defects. If a defect was found, the sample was discarded.

2.1.2 Equipment

This section will review the main equipment used during the research program: the PJET, the high speed camera, thermocouples, microscope, Clima Temperature System (CTS) and the DMA equipment.

Pulsating Jet Erosion Test (PJET)

The PJET developed by DUCOM (Figure 2.2) was used to replicate rain droplets with different impact velocities and frequencies.

Different parameters can be changed while testing. Impact velocity and impact frequency can be changed from the PJET electronic panel. The jet nozzle can be changed to vary the droplet diameter. The air supply can be activated to remove the water film on the sample surface. Table 2.3 summarizes the variables that can be changed and in which range. Before the experimental tests, the PJET impact velocity and frequency were calibrated according

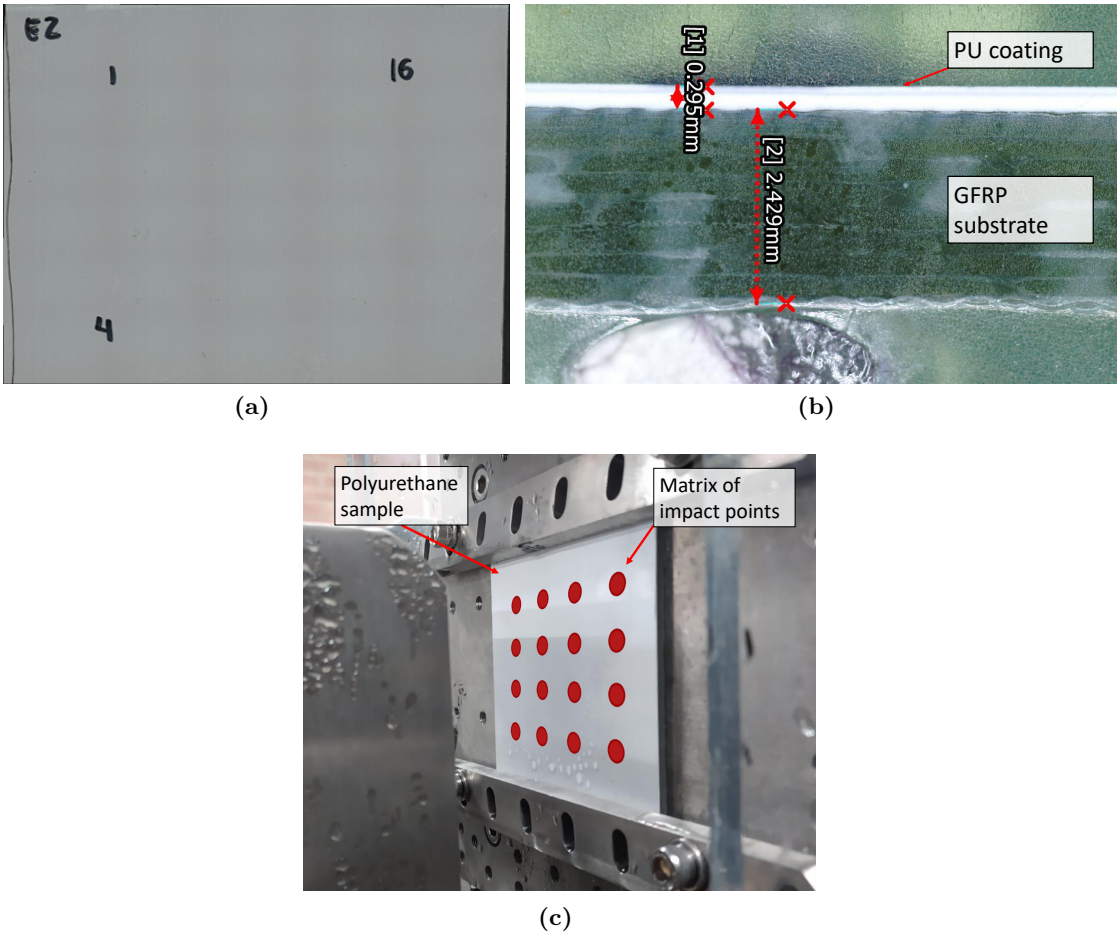

(a) (b)

(c)

Figure 2.1: PU samples that were tested. Figure (a) presents one of the samples after testing. The letter right (E2) refers to the number of the sample. The numbers in the sample refers to the order in which the impacts were carried out. Figure (b) presents the cross-section of one of the samples. This image was obtained with the Keyence microscope (see section 2.1.2). Figure (c) shows the matrix modulation approach with all the tested spots in a single sample.

to its manual. The calibration was carried out three months before the start of the present research project.

Parameter	Range
Impact velocity: v_i	$5 - 250$ m/s
Impact frequency: f_i	$2.3 - 47.4$ Hz
Nozzle size	$0.8, 1.5, 4$ mm
Air supply	ON or OFF

Table 2.3: Testing parameters that can be changed for tests in the PJET.

The PJET jet uses a continuous water jet that goes through a rotating disk with two holes (see Figure 2.3). The water jet gets chopped when passing by the disk, creating a set of water

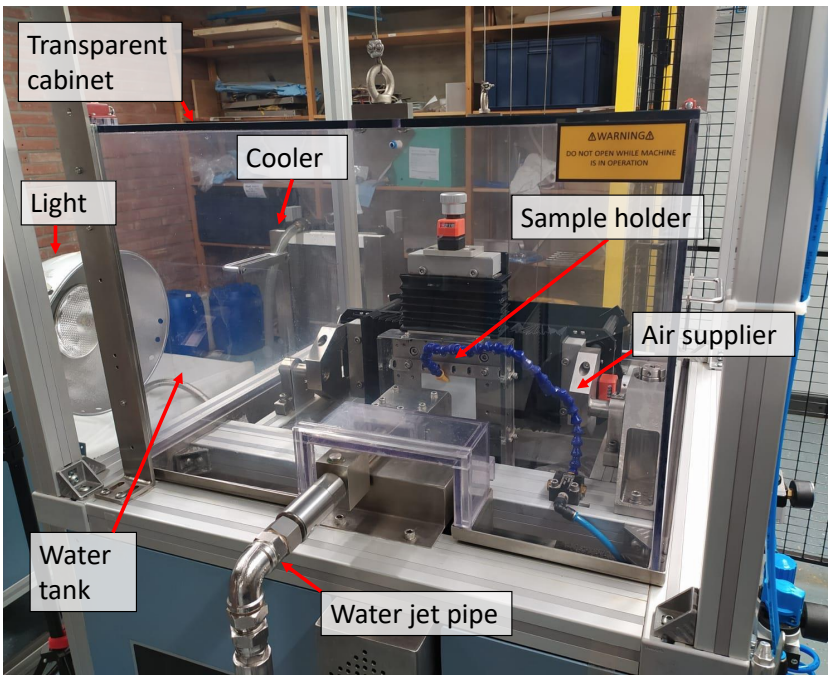

Figure 2.2: DUCOM Pulsating Jet Erosion Tester. The PJET consists and includes several features besides the main equipment: an air supply (or blower) to get rid of the water cushion film on the sample, a cooler to stabilize the water temperature and a water tank that supplies with water to the PJET.

jet segments that simulate rainfall droplets. The change in the rotating disk frequency allows the equipment to change the impact frequency of droplet impacts.

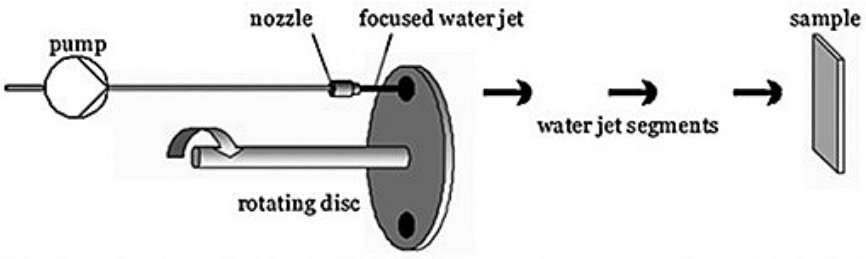

Figure 2.3: Pulsating Jet Erosion Test (PJET) principle. Source: [9]

There are three different nozzles, each of which yields a different droplet size. For the whole research project, the medium nozzle of 1.5 mm diameter was used. This nozzle generates a droplet diameter of approximately 2 mm. This size has been selected as it is one of the most common droplet sizes used in research literature [7]. The reason for this convention is that the droplet of 2 mm is the most probable diameter for heavy rainfall of 25.4 mm/h [41].

The equipment also allows to move the structure to which the sample is attached to change the distance from the nozzle to the sample and to vary the droplet impact angle. For the

whole set of experiments, the distance was set at 50 mm. This distance was recommended by the DUCOM manual to verify that the impact velocity is the one that was calibrated. The impact angle was fixed at 90º to the sample, as this is considered to be the most critical impact angle [38]. The structure where the sample is placed is covered by a transparent cabinet that allowed to see the damage (see Figure 2.2). The transparent cabinet had to remain closed while testing. The cabinet did not include a humidity sensor.

The PJET incorporates an air supply connected to a movable air blower arm (see Figure 2.2) able to remove the water cushion film that may be adhered to the sample after a droplet impact and that may damp the next droplet hit. The air blower pressure can be set up to 2 bar. In literature, values of pressure around 3 bar have been used to remove this water film [10]. Pressure of 2 bar has been used for the air supply in this experiment. A high speed camera was used to check that the air pressure is enough to remove the water cushion that is formed. Figure 2.4 shows the collocation of the blower. The position and orientation of the blower were set based on literature references [10] and based on the high speed footage.

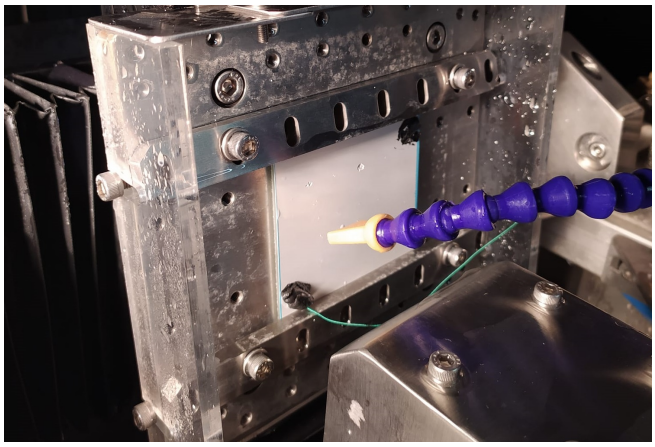

Figure 2.4: Air supply (blower) capable of removing the water cushion on the sample surface.

DUCOM PJET incorporates a cooler that stabilizes the temperature of the impacting water. When the PJET is turned on, the water temperature tends to rise quickly, most probably due to the water going through the PJET pump and the droplets hitting the sample continuously. The cooler helps to stabilize the water temperature. There is not any system to adjust its cooling rate: it just can be turned on or off. This feature implies that the water temperature may get stabilized at different values depending on the testing conditions. Thermocouples were used to ensure that the water temperature measured in the tank remained stable. The thermocouples that were used will be reviewed in the next chapters.

The PJET was used to determine the incubation period of the coatings. The next subsection focuses on the methodology to measure incubation times.

Incubation time determination

The incubation times are defined as the moment when the first damage is visually observed in the sample [29]. The transparent cabinet allowed to observe the samples while testing and spot early forms of damage that indicate mass loss. Lights at the side of the jet were placed

to see the coating damage more clearly. Hydrophobic films were also attached to the cabinet to avoid the condensation of droplets on the cabinet surface and thus, see more clearly the damage. Figure 2.5 show the whole test set-up with all the equipment used.

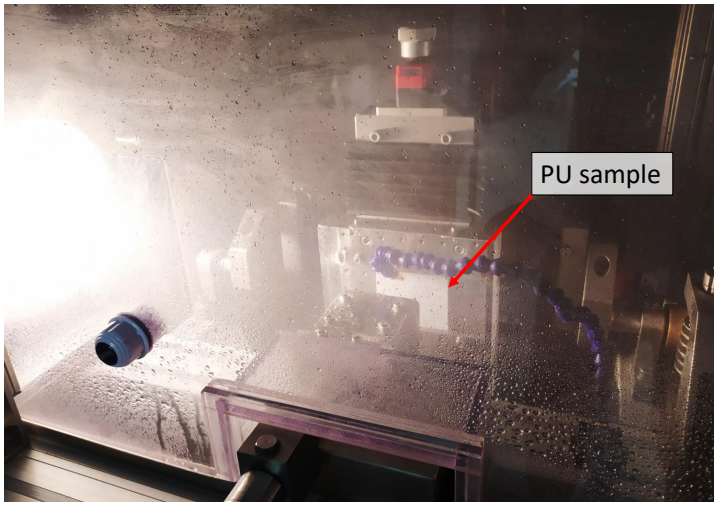

Figure 2.5: Set-up of the PJET equipment while testing. The light allows to see the damage in the tested PU sample.

The way of testing the incubation time is as follows. The PJET is turned on and the impact frequency is set. Then, the impact velocity is raised up to the required value. When the impact velocity is reached, the chronometer is started. Afterwards, the coating is inspected through the cabinet until early damage is observed: this moment is considered the end of the incubation period: the chronometer is stopped and the time is tracked down. After the measurement, the sample is again inspected. If it is considered that the coating is too damaged for the measurement to be considered as an incubation time, the data point is determined unsuccessful and not considered in the final results. Figure 2.1 a) shows an example of a sample with different measurement points. One of the measurements for the incubation time (the upper-left point) was considered failed because the point was too damaged.

The main limitation of the visual inspection through the cabinet is that the damage remains small for some time before getting larger, which means that there is a relatively long range of times that can be considered as valid measurements of the incubation time. An error of ± 15 seconds has been set for these measurements. Furthermore, an error of 15% in the value of incubation time was also considered. This error accounts for the fact that for long incubation times (up to hours), the frequency at which the cabinet was inspected was lower than for short incubation times (around minutes). These two error values have been drawn from general observations while testing.

With this procedure, the total/global testing time is measured. The number of impacts can be obtained by multiplying the obtained global testing time by the impact frequency, which is already known.

High speed camera

A Photron high speed camera (model: FASTCAM Mini AX200, 1 Megapixel resolution) was used to observe the droplet impact phenomena, the shape of the droplet and to examine the water cushion effect: how it is affected by the air supply and for different impact frequencies. Footage of 15000 fps was proven to be enough to observe these effects. High speed footage was obtained for very low velocities (10 m/s approx.) and high velocities (160 m/s). The reason for the selection of these two parameters is that the transparent cabinet can be opened just for very low velocities. For higher velocities, the cabinet should be closed and the high speed pictures are not as clear due to the mist generated. Those two types of footage were used to conclude the water droplet water cushion effect and the droplet shape.

Thermocouples

Thermocouples were used to record the temperatures of the test sample and the water in the tank that supplies the PJET pump. They were used to study the evolution of temperature in time and, to a certain extent, examine if the temperature can affect incubation times values.

Analogical thermocouples type K were used, with alloys of Nickel-Chromium for the positive pole and Nickel Alloy for the negative one. The thermocouple was directly placed at the back of the sample using tape while the thermocouple at the water tank was covered in tape to isolate it from the water (see Figure 2.6). The thermocouple at the sample could not be installed at the coating itself because it was being removed by the lateral jetting. Other systems to measure the temperature (such as IR cameras) were discarded due to the cabinet conditions that included mist and a large number of droplets.

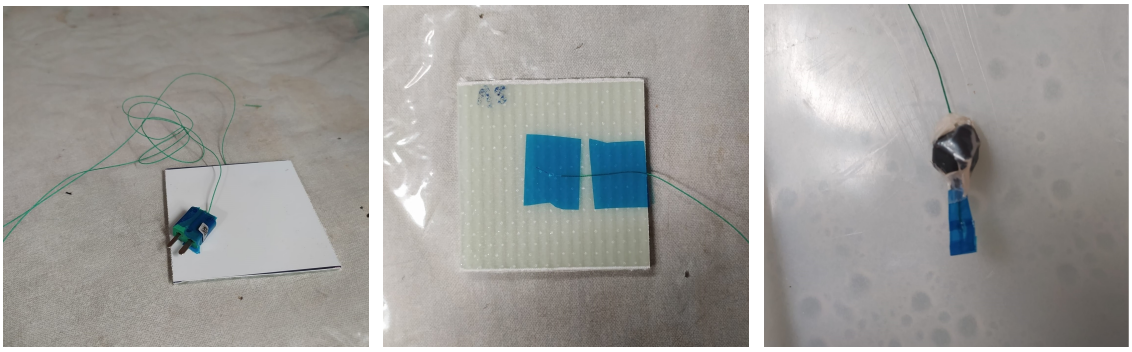

(a) (b) (c)

Figure 2.6: K Thermocouples used in the research project (a). The thermocouple attached to the sample (b) is fixed to the back of the composite substrate. The thermocouple that tracks down the water in the tank (c) has been isolated using tape. This thermocouple is submerged into the tank to measure water temperature.

Both thermocouples showed different error ranges, probably due to the difference in impedances between the GFRP and the water at the tank. The one attached at the sample showed a noise error around $\pm 1°C$, while the thermocouple placed at the noise error of the water tank thermocouple was larger, about $\pm 4°C$. The overall averages of the water tank thermocouple were compared with temperatures measurements carried on with other devices and matched,

validating the continuous temperature measurement of the thermocouples. Both thermocouples were connected to a Keithley Data Acquisition unit was used to gather temperature in real-time. The sampling rate of the temperature was 1 measurement every 10 seconds. This rate was proven to be accurate enough to record the evolution in temperatures.

Stable temperatures were reached for both thermocouples after some time of testing (approximately one hour). This testing time at which temperatures got stable was variable dependant mainly on droplet velocity. For the largest part of the measurements, the water tank temperature was aimed to be stable between 30 and 35 $°C$ after some time. Just the measurements of incubation times in this range of temperatures were considered in the results.

Microscope

The microscope Keyence VR-5000 was used to evaluate the early forms of damage in tested samples (see Figure 2.7). The microscope incorporates a 3D imaging and measurement system able to investigate the height-map of the damaged area. A low magnification (50× on a monitor 15") with wide field of view was used for the general evaluation of the damages. Higher magnification and resolution settings were used to evaluate further specific damage features (80× on a 15" monitor). Height maps were obtained. After setting the base plane in the microscope, the height maps colour palette was set at $[-0.015, 0.015]$ mm. This range enabled a general overview of the damage. The palette was changed to $[-0.004, 0.004]$ mm to observe more subtle changes in some damage features.

Figure 2.7: Keyence microscope.

Damages were compared for different impact velocities and impact frequencies. When investigating the damages, attention was paid into different features:

- Size and nature of the plastically deformed regions.
- Characteristic damage patterns: cracks, pitting or loss of adhesion between substrate and coatings.

Clima Temperature System (CTS)

During the experiments, it was hypothesized that humidity and temperature in the cabinet may affect the incubation times of the coatings. To examine this effect, a Clima Temperature System (CTS model LF7M04, see Figure 2.8) was used to replicate the conditions that were found in the cabinet while testing. The CTS allows for the control of temperature and relative humidity. A commercial ambient humidity and temperature sensor was installed in the cabinet to log the environmental conditions while testing.

Figure 2.8: Clima Temperature System (CTS) equipment.

The CTS was used for three objectives. First, to investigate the water uptake curve of the bulk coating and assess if the coated samples were getting saturated in the cabinet during the tests. Bulk samples were also treated in the CTS to be later tested in the DMA to investigate changes in properties after being subjected to the humidity treatment (see next subsection). Also, the CTS was used to perform humidity samples to coated GFRP until saturated. These saturated (or wet) samples were tested in the PJET to check if there was a difference in the incubation times when compared with coated samples that did not undergo this humidity treatment. The temperature and relative humidity of the CTS was fixed at 38° and 98% RH, values which were considered representative of the PJET testing conditions based on the measurements of the sensors installed at the cabinet.

Samples of bulk coating (see Figure 2.10 a)) were used to obtain the water uptake curve. These samples were first placed in a desiccator for one day to remove all their moisture. Then, the samples were placed in the CTS. Measurements of the weight were carried to elaborate the uptake curve, which was obtained according to the standard ASTM D3574 [42]. The GFRP coated samples that went through the humidity treatment and were to be tested in the PJET afterwards were not placed in the desiccator before the humidity treatment. These coated samples remained in the CTS between one and four days. This amount of time was enough for the coating to get soaked, according to the water uptake curve that was obtained.

DMA

Dynamic Mechanical Analysis (DMA) tests were used to characterize the material and observe if there were changes in the properties of bulk PU samples when varying temperature (using temperature scans) and after undergoing the humidity treatment in the CTS at 38° and 98% RH.

The equipment RSA-G2 Solids Analyzer (see Figure 2.9) was used to perform DMA tests of the bulk coating samples. The samples used are shown in Figure 2.10.

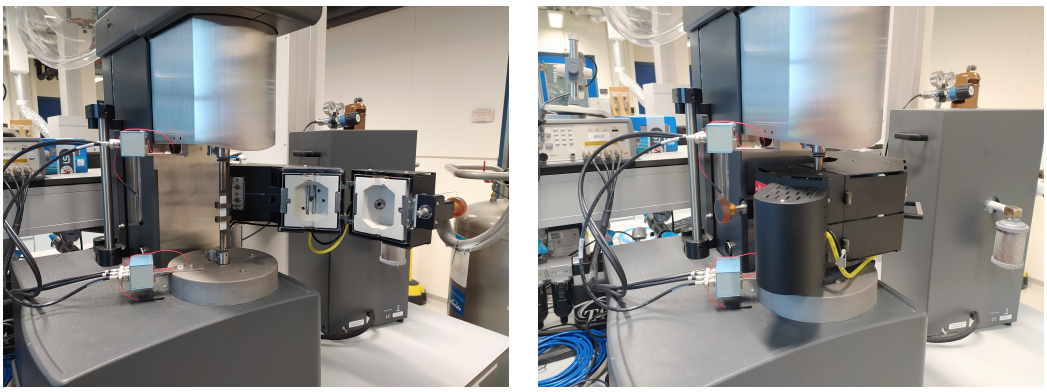

Figure 2.9: RSA-G2 Solids equipment used to carry on Dynamic Mechanical Analysis to the PU coating.

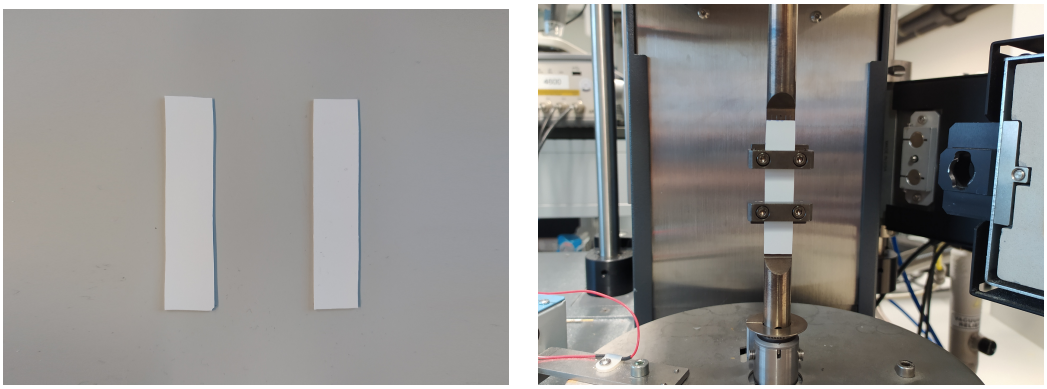

Figure 2.10: Samples DMA. The dimensions range in around 57x2.5mm and 0.5-0.65 mm thickness.

They were subjected to a different set of tests: temperature scans, frequency sweeps and TTS analysis (time-temperature superposition principle, process able to obtain mechanical properties at high frequencies).

Temperature scans, frequency sweeps and TTS analysis (using the time-temperature superposition principle, which enables to obtain mechanical properties at high frequencies) were used to analyze the bulk coating samples. These three analyses have been used in the LEE literature. Temperature scans and frequency sweeps were performed by Ouachan [43] to characterize viscoelastic coatings. TTS analyses have been proven useful when investigating the rain erosion performance of PU coatings. Arena [44] found a correlation between the erosion

mass loss and the storage and loss modulus at high frequency (at $10^7 Hz$) using sandblasting equipment on PU coatings. The properties at high frequencies were obtained via TTS analysis. This value of frequency was obtained with a calculation of the magnitude orders of a typical sand-impact problem. DMA is considered a powerful tool to measure material properties subjected to rain erosion, as the characteristic frequency of high velocity impacts is very high. These high frequencies can be investigated via DMA using the TTS principle [17].

As the bulks samples are very thin (around 0.6 mm), the tensile clamp testing was considered the most suitable setup [45]. The dimensions of the sample were (63 ± 3)x(10 ± 1) mm. The thickness of the tested samples was 0.60 ± 0.05 mm.

Temperature scans were conducted from -10 °C to 100 °C. This range in temperature would include the T_g of the polymer (-5°C) and covers the temperature that was measured in the cabinet while testing. The strain was set at 0.1% (amplitude of 10 µm) at 1 Hz frequency. These values were based on the values of amplitude and initial frequency that were used in the literature to study Leading Edge Coatings [44] [43]. A frequency scan was carried out in the range from 1 to 20 Hz at the same strain and amplitude; the temperature was set at 45°C, which was considered to be close to the actual temperature that the coating may undergo while testing. Although the frequencies used in this scan are much lower than the ones related to high velocity impacts, low frequency scans have been proven to be successful when assessing the change in properties of LEE PU coatings [43]. TTS analyses were performed at 0.5 N static tensile axial load and with a dynamic load of 0.4 N. The range in frequency was set from 0.1 to 1 Hz, and the range in temperature, from $-10°C$ to $70°C$. Reference temperature was set to $40°C$. These values were chosen based on literature [44] [43] and on the temperature measurements that were carried out in the PJET cabinet. The changes of storage modulus (E'), loss modulus (E") and loss tangent ($\tan(\delta)$) were measured. These values are expected to provide useful information about the behaviour of the material.

2.2 Analytical methods

Different methods have been used to analyse the results. The impact frequency tests were plotted in a Wöhler curve and against Springer's model. Probabilistic functions have been used in the early stages of the research project and will be briefly commented on. Factorial and Pareto analysis will also be addressed in this section.

2.2.1 Wöhler curve

The Wöhler curve slope was used to plot the experimental points into Springer's model.

The method presented at the DNVGL recommended practice [46] was followed to estimate the Wöhler curve and present the results. The v_i-n_i curve can be represented assuming a power law.

$$n_i = k \cdot v_i^m$$

The variable n_i represents the number of impacts until incubation time, while v_i is impact frequency. The parameters k and m are the constants related to the material: k is the constant and m represents the slope of the Wöhler curve.

$$log(n_i) = log(k) + m \cdot log(v_i^n)$$

This way, the curve resembles the traditional $S - N$ curves characteristic of fatigue, but impact velocity is plotted instead of stresses, and the number of droplet impacts per site until incubation is plotted instead of the number of cycles.

To know the number of impacts until incubation time, global testing time was measured as stated in section 2.1.2. The number of impacts is obtained by multiplying the average incubation time by the impact frequency (this is, the number of impacts per second). This way, the Wöhler v_i-n_i curve was plotted.

2.2.2 Springer model

The slope of the Wöhler curve (m) was used for the two Springer's models: the one focused on droplet impacts on homogeneous materials, and the one devoted to impact on coated composites [32]. This value has been proven as an essential material parameter to assess the rain erosion performance of coatings [25]. The properties of the coating and the substrate (Tables 2.1 and 2.2) were used for the Springer model. Springer's homogeneous model uses two parameters to obtain the number of impacts until the incubation time of the material: P, which represents the water pressure, and S, which accounts for the effective strength of the material.

$$S = \frac{4\sigma_u(m-1)}{1-2\nu} \tag{2.1}$$

$$P = \frac{\rho_L C_L v_i}{1 + \frac{\rho_L C_L}{\rho_s C_s}} \tag{2.2}$$

Springer's homogeneous model predicts the number of impacts until incubation time with these two values, given by the equation:

$$n_i^* = 7.1 \cdot 10^{-6} \cdot \left(\frac{S}{P}\right)^{5.7} \tag{2.3}$$

Springer's coated composites model takes into account the number of reflections between the substrate and the coating. The parameters that predict the number of impacts until incubation are equivalent to the ones in the homogeneous model, but to account for these effects: the strength parameter S_e now substitutes S, and the mean stress at the liquid-coating interface σ_0 replaces the stress P. The formulation of these parameters can be read at Springer's work [47].

$$n_i^* = 7.1 \cdot 10^{-6} \cdot \left(\frac{S_e}{\sigma_0}\right)^{5.7} \tag{2.4}$$

Both Springer's models, homogeneous and coated, rely on assumptions. Those are mainly:

- For the homogeneous model, the number of impacts until incubation time (n_i) is supposed to be more than one. This assumption is mathematically expressed:

$$\frac{S}{P} > 8 \tag{2.5}$$

- The same assumption is made for the coated model:

$$\frac{S_e}{\sigma_0} > 8 \tag{2.6}$$

- For the homogeneous model, there is a minimum thickness at which no reflections will occur. The homogeneous model does not consider stress reflections, so this equation should be satisfied. C_C and C_L are the speeds of sound in the coating and the material.

$$h_c > 2d_d\frac{C_C}{C_L} \tag{2.7}$$

- The coated model accounts for reflections in the coating, but not in the substrate. The substrate should be thick enough for this assumption to be true, so the following equation should be satisfied.

$$h_s > 2d_d\frac{C_S}{C_L} \tag{2.8}$$

- The coated Springer considers that the interphase between the coating and the substrate is perfect, that stresses and deformations are equal at both sides of the interphase. These assumptions will be reviewed after the application of Springer's model.

2.2.3 Probabilistic distribution

Probability distributions have been used in the early stages of the project. The objective was to find a good probability distribution fitting for initial measurements of incubation times.

To assess the fit of a probabilistic plot, different tools have been used. The p-value is a probability that measures the evidence against the null hypothesis, being the null hypothesis (H_0), in this case, that the data follow the distribution [48]. Low p-values provide evidence that the data does not follow the distribution. The p-value can be compared with the significance level (α), which accounts for the risk of stating that the set of data does not follow the distribution when it actually does. The significance level is usually set at 0.05. If p-value$< \alpha$, it can be concluded that the data do not follow the distribution. On the contrary, if p-value$> \alpha$, it can be assumed that the data follows the distribution.

Probably plots have also been used to assess the fit of the probability distributions. Those plots display the data point with its percentage of values in the data that are less to it [48]. The data points should be approximately in a line between confidence lines.

Those two methods have been used to assess the fir of probabilistic functions to data. In the case of this work, it was found that the best fit was the lognormal function. This function is defined by two parameters: the mean ν and standard deviation σ [49]. The mode, median and mode of the lognormal function have the following expression:

$$Mean = exp(\mu + \frac{\sigma^2}{2})$$

$$Median = exp(\mu)$$

$$Mode = exp(\mu - \sigma)$$

2.2.4 Factorial analysis

A general full factorial analysis has been used in the present work to post-process the results related to the second Research Question of this work: the influence of the input dry interval parameters (λ, α and β) over the output ratio r (see more in following sections).

The factorial analysis allows to know which parameters contribute the most to the variability of the response [50]. The Pareto chart was used for that regard, comparing the relative magnitude and the statistical significance of the main effects. A confidence interval of 95 % was used for the analysis ($\alpha = 0.05$). The analyses yield the absolute value of the standardized effects. If this value is larger than the reference line, the parameter is considered statistically significant. The reference line is drawn using Lenth's method, based on sparred factor effects, which assumes that the variation in the smallest effects is due to random error [51].

To further assess the significance of the parameters, p-values were used. The p-values for each term were compared with the significance level ($\alpha = 0.05$). If the p-value for a term is lower than α, the association between this term and response is statistically significant; if not, it cannot be concluded [50]. The trend in which the factors affect the response (ratio r) was evaluated with the main effects plot [52].

2.3 Test Plan

The main part of the experiments has been performed using the PJET. After those tests were performed, an evaluation of the damage was carried out. As stated in previous sections, PU samples were subjected to humidity treatment in the CTS until got saturated. These samples were then subjected to DMA for material characterization.

2.3.1 PJET tests

The test plan was divided into several parts. First, experiments were performed to study the effect of the water cushion for different impact frequencies and a fixed velocity. The next set of experiments examined the incubation times for different impact frequencies and velocities. This experimental data was compared with the Springer model. Finally, experiments were carried out to know the effect of performing dry intervals while testing and if there is a change in the incubation times. The impact velocity and frequency were fixed for this last set of experiments.

Water cushion study

This set of experiments aims to determine the effect of different impact frequencies and the removal of the water film on the incubation times in the polyurethane coating. These experiments will also shed light on the effect of impact frequency just for this velocity.

Tests were performed both with the air supply on or off (see picture 2.4). Three impact frequencies were examined: 2.5 Hz, 27.7 Hz and 42.6 Hz. These frequencies have been selected as they cover the whole range of frequencies allowed by the PJET. However, as explained in previous chapters, they are not representative of the real-life raindrops impact frequencies [8]. These three main frequencies have been used during the whole research project and will account for low, medium and high impact frequency.

f_1	f_2	f_3
2.5 Hz	27.7 Hz	42.6 Hz

Table 2.4: Droplet impact frequencies used to examine its effect on incubation times.

The impact velocity was fixed at 160 m/s (±2 m/s). The impact velocity was selected as a very high velocity may damage and rupture the samples too quickly and a low velocity would increase the testing time.

A total number of 66 measurements were taken with the air supply off, and 75 measurements were taken with the blower on. Table 2.5 shows the number of data points that were measured for each impact frequency. This data was fit into a probabilistic function. Based on the shape of the distribution of the results, four probability distributions were fit: normal, lognormal, Weibull and gamma distributions. The p-values of each distribution are compared with the significance level to assess the fit of the distribution. A significance level of $\alpha = 0.05$ has been used. This level implies that the risk of deciding that the data does not follow the distribution when, actually, they follow the fit, is 5 %. If the p-value is less than the confidence level (0.05), the data is not considered to follow the distribution. If the p-value is larger than the confidence interval, it cannot be concluded that the data do not follow the distribution. After examining the probabilistic distributions, it was considered accurate to use the means of incubation times to compare the effect of the impact frequency for other impact velocities. Then, from that moment on, means were used to evaluate the incubation times for the rest of the tests.

f_i (Hz)	2.5	27.7	42.6
Air supply: ON	26	23	26
Air supply: OFF	20	20	26

Table 2.5: Number of measurements for each combination of impact frequency and state of the air supply.

During this set of tests, the temperature of the sample and the water tank were measured using thermocouples. The values of incubation times were considered valid just when the water temperature remained stable around $33 - 36°C$. The experiments in which the water temperature was outside this margin were discarded.

Impact frequency tests

The aim of this set of experiments is to know the change in incubation times when varying the droplet impact frequency and impact velocities. Experimental data points led to the Wöhler curve. Then, data points were plotted against the Springer model.

Five impact velocities (see table 2.6) and the three impact frequencies (see table 2.4) were evaluated. A matrix modulation approach was used: the coated sample was divided into distinct matrix points, each of them tested with a different impact velocity and frequency (see Figure 2.1 c). The air supply was aiming at the sample during all the tests of this set to remove the water cushion. This situation is more comparable to a real-life situation in a wind blade, where high velocities remove the cushion [23].

v_{i1}	v_{i2}	v_{i3}	v_{i4}	v_{i5}
130 m/s	140 m/s	150 m/s	160 m/s	170 m/s

Table 2.6: Droplet velocities at which incubation times were examined. For the lowest velocity (130 m/s), just one measurement was performed due to time constrains.

During the tests, a high deviation of the results was noted. To detect and discard outliers, two filters were used. The first filter accounted for environmental situations (that the water temperature remained in a range of $33 - 36°C$). A second filter focused on statistical outliers. This statistical filter considers a data point as an outlier when this point is 3 Median Absolute Deviation (MAD) away from the mean. Other configurations for the statistical filter were tested (based on quartiles rather than in the MAD), but the filter performance was pretty similar. Table 2.7 displays the number of measurements that were taken into account after applying the filters.

$f_i \setminus v_i$	130 m/s	140 m/s	150 m/s	160 m/s	170 m/s
2.5 Hz	1	2	7	20	8
27.7 Hz	1	2	7	22	24
46.7 Hz	1	5	5	19	5

Table 2.7: Number of measurements that were taken for each combination of impact frequency and velocity. Environmental and statistical filters to remove outliers were considered. Note that for 130 m/s just one point was measured for each impact frequency.

The relatively small amount of experimental data per point does not allow for the development of a statistical fit of incubation time (as it was done for the previous set of experiments when the water cushion effect was studied). To analyze the incubation times now on, the means of the measured data points were taken. These means were used to estimate the Wöhler curve.

The Wöhler curves were obtained according to the DNVGL procedures [46]. The slope of the curves, m, was estimated. Then, the data points were plotted into the Springer model.

Dry interval tests

The objective of this set of experiments is to determine the effect of the dry intervals on the incubation times. The impact frequency was fixed at 27.73 Hz. This value was chosen as it

is the medium value of frequency that was previously tested. Furthermore, similar values of impact frequency have been used in past PJET tests in the literature [10]. Velocity was set at 160 m/s. This value is not too high to prevent drastic rupture of the coating. At the same time, for this impact velocity, the incubation times do not take too long and can be achieved in a reasonable amount of time.

To define the dry intervals, three parameters were defined: λ, α and β. These parameters define the duration of the dry interval (t_{dry}), the moment at which point the dry interval starts ($t_{dry\,0}$) and how many pauses there are. These magnitudes that define the dry interval are based on the reference incubation time, $t_{i\,(ref)}$, which was found when dry intervals were non-existent. The three dry intervals parameters are:

- λ: specifies the duration of the stop when compared with the reference time. It is defined as the fraction between the duration of the dry interval (t_{dry}) and the duration of the original incubation time ($t_{i\,(ref)}$)

$$\lambda = \frac{t_{dry}}{t_{i\,(ref)}} \tag{2.9}$$

- α: defines when the stop begins. It is defined as the fraction between the time at which the dry interval starts ($t_{dry\,0}$) and the duration of the original incubation time ($t_{i\,(ref)}$)

$$\alpha = \frac{t_{dry\,0}}{t_{i\,(ref)}} \tag{2.10}$$

Figure 2.11 shows several examples of how these parameters define and characterize the dry interval.

The dry intervals are completely defined by these three parameters: their duration, when the interval starts and how many stops there are. Two values were chosen for each parameter, yielding a experimental matrix of 8 cases. The values for the parameters are shown in table 2.8. The choice of these values was to have a general impression of the phenomena that could happen in a real-life rainfall situation, where several pauses of different duration can take place.

Parameter	λ	α	β
Value 1	1	0.2	1
Value 2	5	0.5	5

Table 2.8: Values for the parameters that characterize the stops while testing: λ, α and β

The reference incubation time has been considered as the one yielded by the previous set of experiments. Due to the high dispersion of the results, some measurements of the reference incubation time ($t_{i\,(ref)}$) were carried out during the stop tests. This way, it could be assured that the reference incubation time is stable and that any change in the incubation times is because of the stops.

The change in the incubation time was tracked using a ratio (r), the dependent variable for this set of experiments. It is defined as a fraction between the incubation time without stops

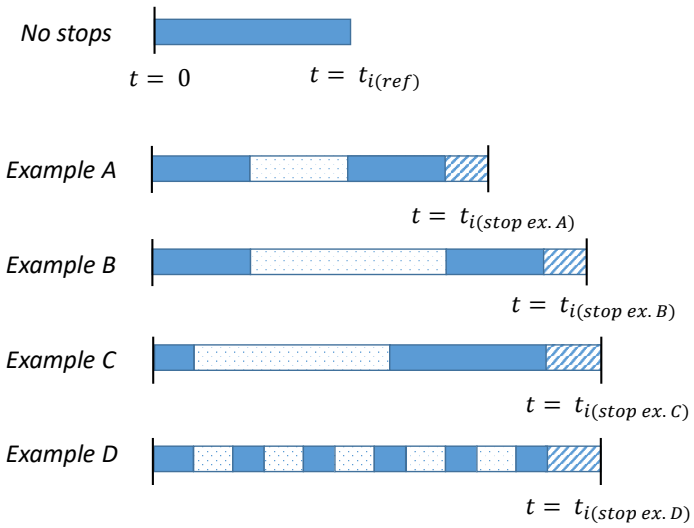

Example	λ	α	β
A	0,5	0,5	1
B	1	0,5	1
C	1	0,2	1
D	1	0,2	5

Figure 2.11: Four examples that illustrate the impact of λ, α and β in the dry interval. The coloured area represents the time at which the PJET is on. The white-dotted area shows the time at which the test was stopped. The striped area shows the change in the incubation time that may be expected and will be evaluated.

$(t_{i\,(ref)})$ and the incubation time value obtained during the stop tests $(t_{i\,(stops)})$. The formula below shows the expression for the ratio. A ratio of 1 would mean that the incubation time has not changed at all when dry intervals are performed. A ratio higher than 1 would mean that the incubation time has increased. Note that for this set of experiments, the impact frequency is fixed at 27.7. Then, testing time and number of impacts until incubation time are always proportional for every case: evaluating the incubation time (t_i) is the same that evaluating the number of impacts until incubation (n_i).

$$r = \frac{t_{i\,(stops)}}{t_{i\,(ref)}} \tag{2.11}$$

The values of the ratio r were studied with factorial analysis to know the influence of the different dry interval parameters. Temperature and humidity were controlled as in the previous set of experiments.

Chapter 3

Results

The present chapter will address the results of the research project. First, the aspects that may have an influence on test results that were investigated are addressed. Then, the experiments that answer the two main research questions are presented: tests that investigate the influence of impact frequency and the performance of dry intervals while testing.

3.1 Erosion test parameters

Three parameters were investigated that could change the incubation times when determining the influence of the impact frequency and dry intervals on them. Those are the water cushion effect, temperature and humidity conditions.

3.1.1 Water cushion

The effect of the water cushion phenomena was examined for high-speed velocities (160 m/s) and for three different impact frequencies (2.7 Hz, 27.7 Hz, 42.6 Hz). High-speed footage for low velocities (10 m/s) was used to validate the removal of the water cushion film. Figures 3.1 show the moment of droplet impact on the coated sample for two different impact frequencies (2.7 Hz and 42.6 Hz) with the air blower on and off.

The water cushion effect appears clearly for high droplet impact frequencies (42.6 Hz) when the air supply is not active. It appears in a more subtle manner for low impact frequencies (2.7 Hz) then the air supply is inactive. The water cushion is not observed at all when the air supply is active, regardless of the impact frequencies. This observation suggests that the water cushion was effectively removed by the air supply.

Figure 3.1 show high speed pictures taken for very low velocities. The water cushion removal could not be verified for higher velocities due to the limitations of the equipment: the transparent cabinet and mist created did not allow to see the coated sample high velocity (see

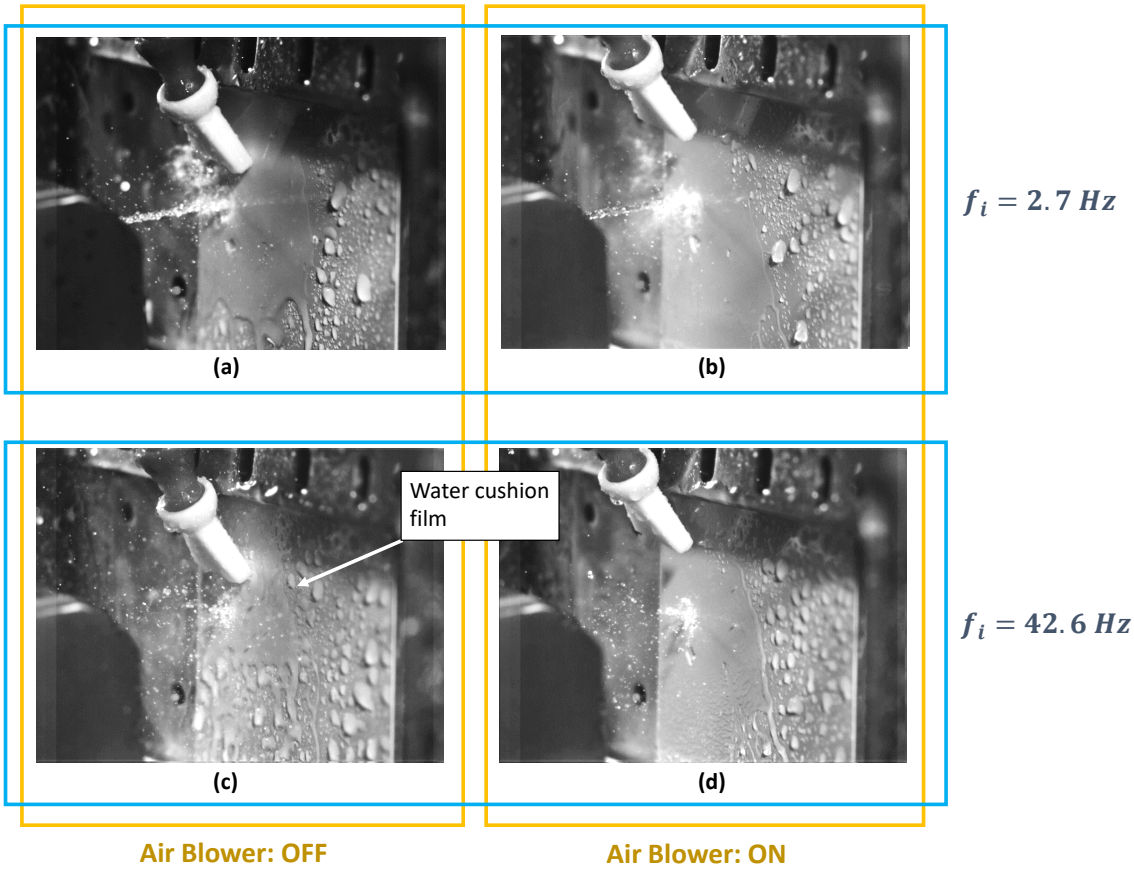

Figure 3.1: High-speed footage showing the moment of impact for different impact frequencies and with the air supply active and inactive. Images a) and b) show low frequency, images c) and d) present high frequency impacts. Images a) and c) do not the air supply active, while it is active in b) and d). The water cushion film can be observed for high impact frequency with the air supply off (case c), and it is more subtle for low frequency with the supply off (case a). With the air supply on, the water cushion is removed.

Figure 2.5). For higher velocities, water cushion effects are expected to be less severe: lateral jetting velocities will be faster and the water cushion will go away more quickly.

Once the effect of the air supply on the water cushion effect was studied, the incubation times were measured. Table 3.1 summarizes the p-values for every studied probability distribution and for every case.

The highest p-values were found in every case for the lognormal function when compared with the rest of the fits. For all the lognormal fits, the p-value obtained is higher than a significance level of $\alpha = 0.05$. The probability plots for the different distribution plots were also examined: the experimental points are expected to form a line within the confident value lines ($\alpha = 0.05$). Probability plots of the lognormal fit are shown in Figure 3.2.

All experimental data points fall within the confidence interval in the probability plots when considering the lognormal fit. This fact, as well as the p-values from Table 3.1, indicate that the lognormal fit is accurate enough to be used [48]. Lognormal fits are now used to investigate the effect of the water cushion effect.

	Air supply: OFF			Air supply: ON		
Fit:	2.5 Hz	27.7 Hz	47.7 Hz	2.5 Hz	27.7 Hz	47.7 Hz
Normal	0.009	0.024	0.018	<0.005	<0.005	<0.005
Lognormal	0.193	0.865	0.188	0.068	0.872	0.223
Weibull	0.091	0.193	0.081	<0.010	0.158	0.024
Gamma	0.101	>0.250	0.110	0.015	>0.250	0.049

Table 3.1: P-values for every probabilistic distribution used to fit the data from the water cushion study.

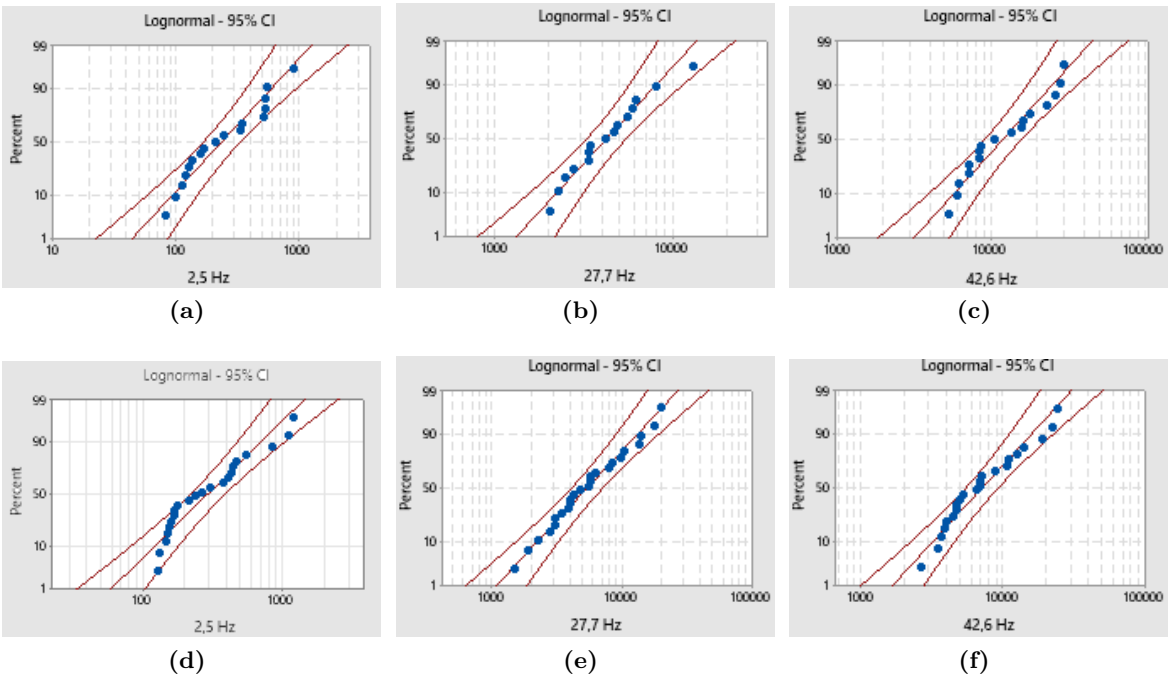

Figure 3.2: Probability plots of the lognormal distribution for every case tested. The upper row presents the data with the air supply inactive, while the bottom row presents data with the air supply on. Impact frequencies: 2.5 Hz (sub-figures a) and d)), 27.2 Hz (sub-figures b) and e)) and 42.6 Hz (sub-figures c) and e)).

Figures 3.3 show the lognormal fits for the three impact frequencies when the air supply is active and inactive. A shift in the fit can be observed when changing impact frequency: when the impact frequency is reduced, the number of impacts until incubation time diminish. Another shift related to the air supply can be observed by observing the lognormal plots: when the air blower is active (and then, the water cushion was removed), the number of impacts until incubation is slightly reduced but just for the case of high impact frequencies (42.6 Hz)

The lognormal fit has three features that can be used to compare them: the mean, the median and the mode. These parameters are used to assess the influence of the water cushion effect and impact frequencies.

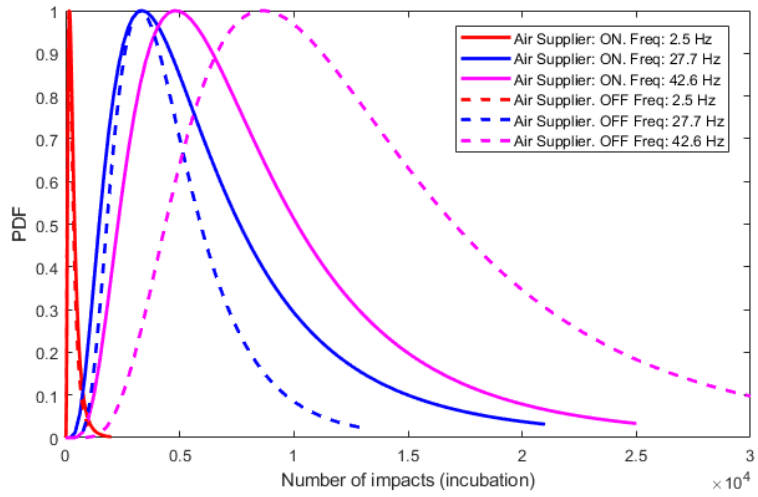

(a)

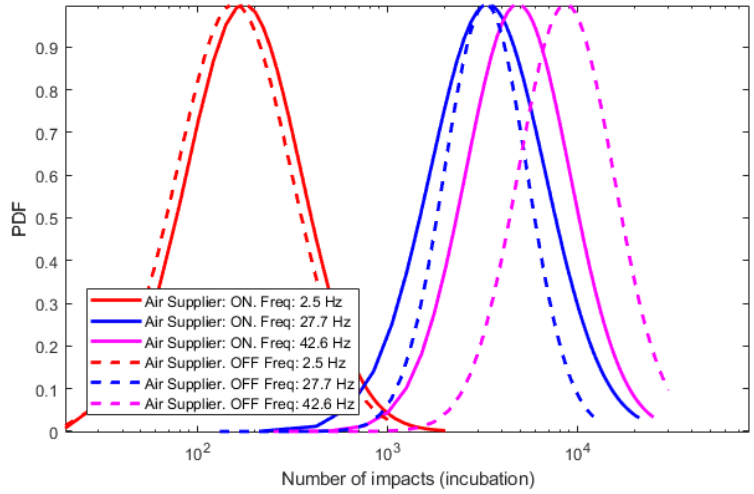

(b)

Figure 3.3: Lognormal fits for the experimental data of number of impacts until incubation. The impact frequency and air supply status (ON or OFF) are considered. The data has been plotted in a linear axis (a) and lognormal axis (b).

Table 3.3 reviews the change in percentage for the mean, median and mode of the lognormal fits when the air supply is inactive (and then, water cushion effect may exist), and compared with the case with no water cushion at all (air supply active). An increase is observed in all the parameters for higher frequencies (42.6 Hz) when there may be water cushion: all lognormal parameters were raised about +60 to +80%. It also shows a decrease in these parameters for the lower frequencies: about −30% for 27.7 Hz and about −10% for 2.5 Hz.

The effects of the impact frequency were evaluated based again on the mean, median and mode. Table 3.3 shows the change in percentage for the mean, median and mode of the lognormal fits for the three impacts frequencies. The medium frequency (27.7 Hz) has been

f_i	Mean	Median	Mode
2.5 Hz	-10.9	-11 1	-11.4
27.7 Hz	-31.3	-22.8	-2.4
42.6 Hz	+62.4	+67.7	+79.0

Table 3.2: Effects (%) in the mean, median and mode of the lognormal fits when there air supply is active is (no water cushion effect). The reference has been set for the case when the air supply is not active (and thus, the water cushion effect may exist).

chosen as a reference. The table shows a tendency: when impact frequency (f_i) is reduced, the mean, median and mode decrease; when impact frequency is increased, those values rise. All the lognormal parameters (mean, median and mode) correlate this trend.

f_i	Mean	Median	Mode
2.5 Hz	-94.84	-94.82	-94.79
47.6 Hz	25.84	31.61	43.96

Table 3.3: Effects (%) in the means, medians and modes of the lognormal fits for the number of impacts until incubation time. Effects vary depending on impact frequency. The medium impact frequency ($f_i = 27.7Hz$) has been set as reference.

It was noted that, although the number of impacts until incubation time was influenced by the impact frequency, the testing time until incubation (this is, the time at which the experiment was held until damage in the acting was observed) was very similar for all frequencies. This fact is summarized in table 3.4, which shows the average and standard deviation of the number of impacts until incubation (n_i) and testing time until incubation (t_i) for every frequency. It can be observed how the testing times are comparable among frequencies, but the number of impacts is not.

f_i	2.5 Hz	27.7 Hz	47.6 Hz
n_i	364 ± 296	6902 ± 4981	8790 ± 6089
t_i (s)	147 ± 119	249 ± 180	206 ± 143

Table 3.4: Comparison between number of impacts until incubation time (n_i) and global testing time in seconds (t_i) for different impact frequencies (impact velocity: 160 m/s). Case: air supply active (no water cushion).

When performing this set of experiments, it was noted that environmental temperature may play a role in the values of n_i. Their effects were investigated.

3.1.2 Temperature

It was noted that incubation times tended to increase at the beginning of the day and were decreasing over time throughout the day and converged after some measurements. This effect was also observed after stopping the PJET for some time: when coming back to the test equipment, incubation times were higher. Figure 3.4 illustrates this trend, showing the global

testing time until incubation (t_i) for different measurements carried out during the day. This magnitude, t_i, had already been shown to be similar for different impact frequencies in table 3.4. Each colour line represents a day in which these measurements were taken, and the x-axis represents the order in which those were recorded. It can be seen how the incubation time is high at the beginning of the day, and then it drops until it converges to a certain value. This trend was observed every time when PJET tests were carried out and for all impact velocities and frequencies.

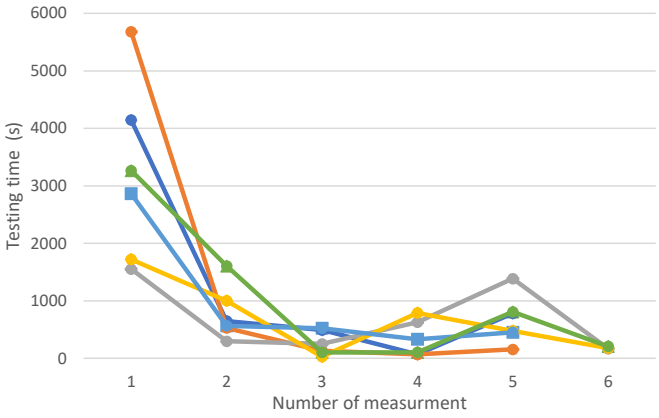

Figure 3.4: Evolution of the value of global testing time (t_i) throughout the day. The x-axis represents the order in which those measurements took place. Each color line represents a different day. All impact frequencies were considered, as their t_i values are comparable (see Table 3.4). Impact velocity: 160 m/s.

It was hypothesized that temperature was playing a role in this phenomenon. Thermocouples were installed to measure the temperature at the water tank and in the sample. Figure 3.5 (a) and (b) show the characteristic profiles in temperature measured with the thermocouples. The Figure at the left (a) presents the temperature of both the water and sample at the first measurement of the day. The Figure at the right (b) presents its evolution for the next measurement. The water at the beginning of the day (a) was at 20°, while the temperature for the next measurement was already stable at $33 - 36$°C. During the rest of the tests of the day, the temperature remained stable in this range. It was observed that about 30 minutes were needed for the temperatures to be stable. Both temperatures (water tank and sample) had very close values when stable. The trends showed in Figure 3.5 were observed for all impact frequencies and velocities.

The effect of the water tank temperature on the incubation times was investigated. The average of the temperature profile recorded while testing (as shown in Figure 3.5) was calculated for each measurement. The global testing times that were obtained were plotted against these average temperature values. The scatter plots that were obtained are shown in Figures 3.6, each of them focused on one impact frequency. The impact velocity was set at 160 m/s.

A power law was fitted for the scatter plots of Figure 3.6. The significance of these fits was checked with the R-Square and the p-values. Table 3.5 shows these two parameters, as well as the significance obtained with the regression. The p-value is used to know the significance of the relationship. If the p-value is lower than the significance level, the correlation is statistically significant, and that the null hypothesis (H_0) (which supposes that the means for

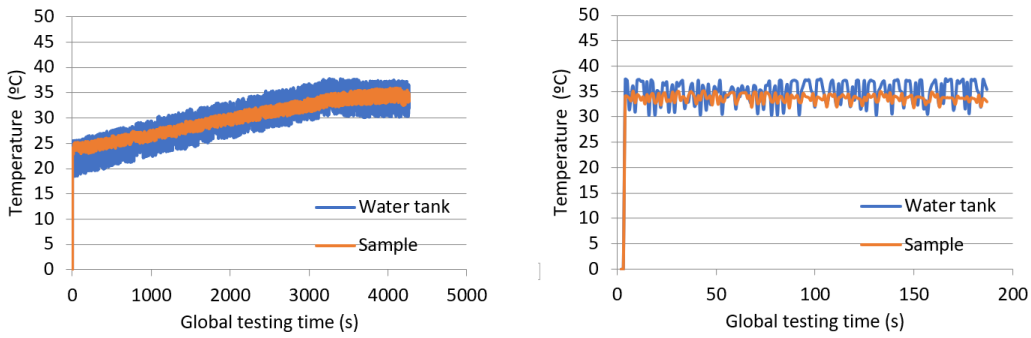

Figure 3.5: Evolution of the temperature of the sample and the water tank while testing. Figure (a) presents the evolution in temperature for the first test of the day. Figure (b) shows the temperature evolution for the second test of the day. Temperature is plotted on global testing time (this is, the time that the PJET was active). Impact velocity: 160 m/s.

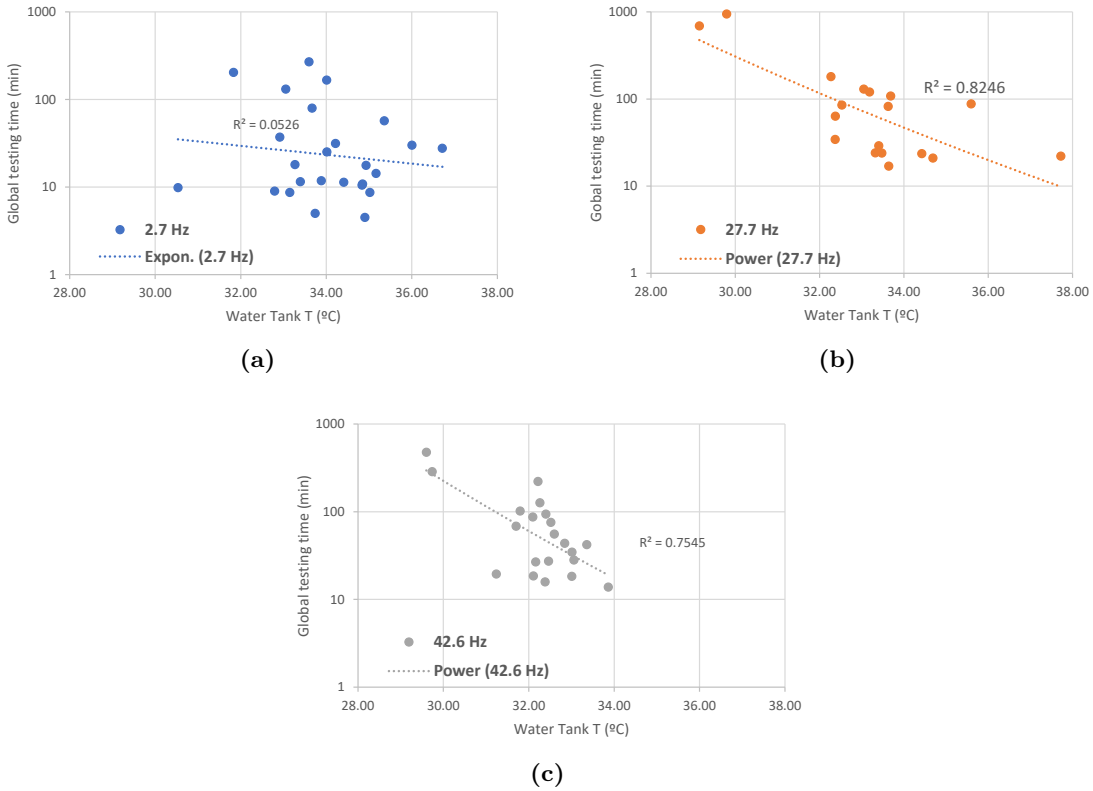

Figure 3.6: Influence of average water temperature on the global incubation time (t_i). On the x-axis, the average water temperature. On the y-axis, the global time that the testing lasted until the incubation time. Three frequencies were addressed: 2.7 Hz (a), 27.7 Hz (b) and 42.6 Hz (c) at 160 m/s.

each level of the temperature are the same), is not a good model [53]. The significance level was set to $\alpha = 0.05$.

f_i (Hz)	2.7	27.7	42.6
R-square	0.053	0.825	0.754
p-values	0.528	<0.001	<0.001
Significance	No	Yes	Yes

Table 3.5: R-squared and p-values for the correlation between water temperature and incubation times (see figure 3.6). Level of significance: $\alpha = 0.05$

Figure 3.6 and the results from table 3.5 show that water temperatures may have an effect on incubation times. A significant effect was found for high frequencies (27.7 and 42.6 Hz), but not for low frequencies (2.5 Hz). The experimental points in Figure 3.6 show that there are some clusters and some distant points that may point out towards the obtained correlation. The correlation cannot be discarded, but other phenomena may have also caused the drop in incubation times over the day, such as humidity.

3.1.3 Humidity

A humidity sensor was installed inside the transparent cabinet. Before turning on the PJET, the humidity in the cabinet is about 40-50 %. When the PJET is turned on (as well as the cooler), the continuous droplet impacts on the sample create mist and the environment in the cabinet gets very humid (see Figure 2.5). The humidity increases very quickly for all impact velocities and frequencies, and remains stable around 95% after just some minutes. For higher impact frequencies the mist is more noticeable for higher impact frequencies, probably due to the higher number of impacts and mini-droplets ejected.

First, the water uptake curve was obtained with bulk coating samples. Figure 3.7 shows the water uptake curve.

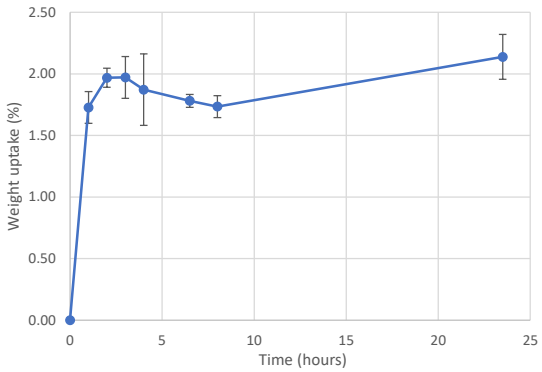

Figure 3.7: Water uptake of the polyurethane coating measured as a fraction of the original sample weight.

The water uptake curve shows that the PU bulk coating absorbs water very quickly and then remains mostly stable. Coated samples were placed in the CTS to undergo a humidity

treatment until saturated and check if the incubation times were changed when tested in the PJET. These are the so-called "wet samples". Figure 3.8 shows the evolution in the measurements of global incubation times (t_i) for these saturated wet samples during the day. These measurements were compared to the same plot for dry samples which were not treated in the CTS (Figure 3.4. These two graphs have been summarized in Figure 3.9. The average and deviation are shown for both cases: the dry and wet (saturated) samples.

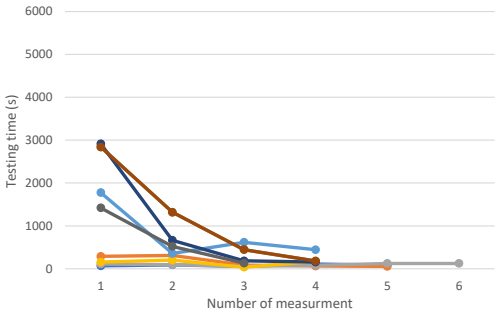

Figure 3.8: Evolution of the global testing time (t_i) throughout the day for "wet samples" which went through the humidity treatment at the CTS. The x-axis represents the order in which those measurements took place. All impact frequencies were considered, as their t_i values are comparable (see Table 3.4). Impact velocity: 160 m/s.

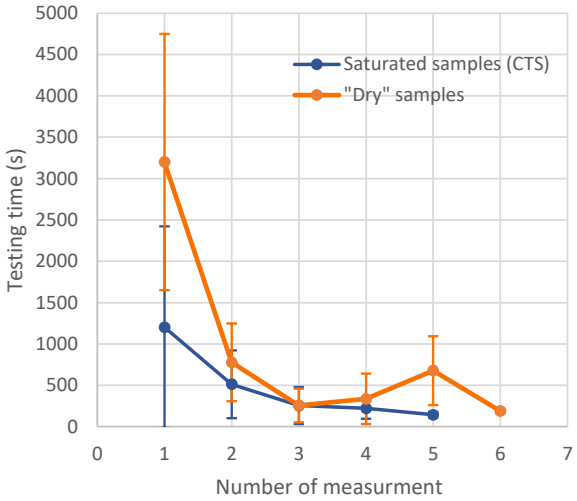

Figure 3.9: Comparison between the evolution in global testing time until incubation (t_i) for dry samples (not CTS-treated) and wet saturated samples (CTS-treated). The x-axis represents the order in which those measurements took place. All impact frequencies are considered. Velocity: 160 m/s

Figure 3.9 shows that the initial incubation times for wet samples at the beginning of the day was lower than for dry samples. However, an initial peak at the beginning can still be observed. For both cases, incubation times converge to a certain value after some measurements. CTS samples converge more rapidly than dry samples.

DMA analyses (temperature scan, frequency scan and TTS analysis) were carried out to know the influence of the saturation in the mechanical properties of the coating.

The temperature scan is shown in Figure 3.10. The plot shows that when increasing the temperature, there is a drop in the storage modulus (E') and loss modulus (E") of bulk coating (both dry and wet samples). When considering the range in temperatures from 30 °C to 70 °C, the E' drops from 60 MPa to 6 MPa, while the E" is reduced from 8 MPa to 1 MPa. This temperature range (30 °C-70 °C) was chosen because it can correspond to a situation of the coating be locally heated at the impact point. Storage and loss moduli do not seem to change when comparing wet and dry samples. The only change between wet and dry samples is in the tan(δ): the plateau of the tan(δ) shifts to the left when the sample is wet, when for the dry sample the plateau is around -5 °C.

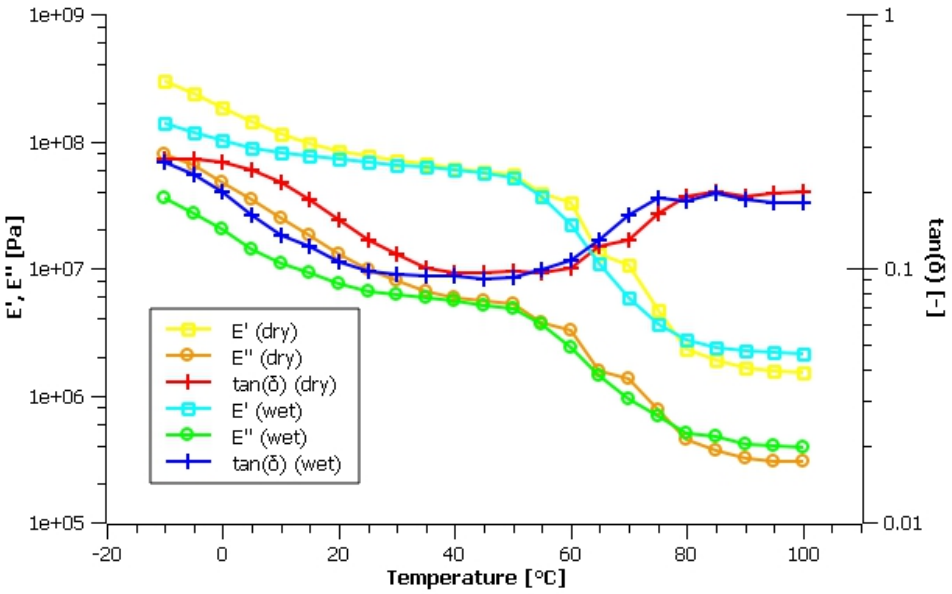

Figure 3.10: Temperature scan analysis for dried and saturated samples.

The frequency scan is shown in Figure 3.11. It shows a slight decrease of the storage modulus and loss modulus (about -25%) for the wet samples when compared with dry samples. No differences in tan(δ) were reported.

TTS analysis is shown in Figure 3.12. This analysis compares dry and wet samples for higher frequencies (the ones that are expected from a high-velocity impact problem). The storage modulus is superior to the loss modulus for all the frequencies, a feature that is also observed in other polyurethane coatings [44]. Attention will be paid to the value of frequency $1e7$ Hz, as this value is suggested by literature to be related to high velocity problems [44]. For this frequency, the storage modulus E' drops from 400 MPa to 150 MPa when saturated, and the loss modulus E" goes from 90 to 40 MPa. This drop is higher for high frequencies than for low frequencies: this may be the reason why this decrease in properties was not seen in the temperature sweep (Figure 3.10).

3.1.4 Summary

In this section, some variables that may play a role when measuring the incubation times have been discussed: the water cushion effect, the temperature and humidity. These variables

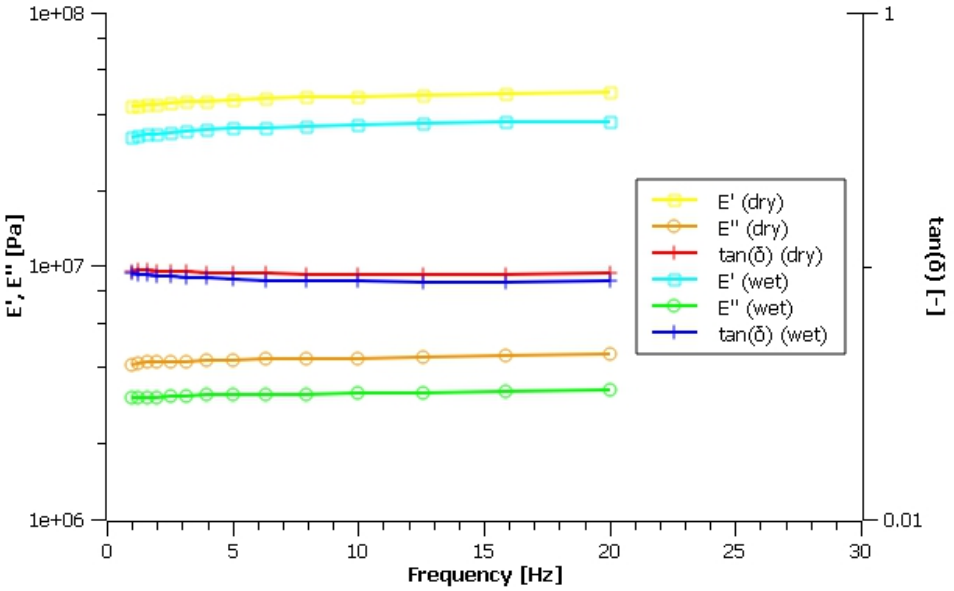

Figure 3.11: Frequency sweep analysis for dried and saturated samples.

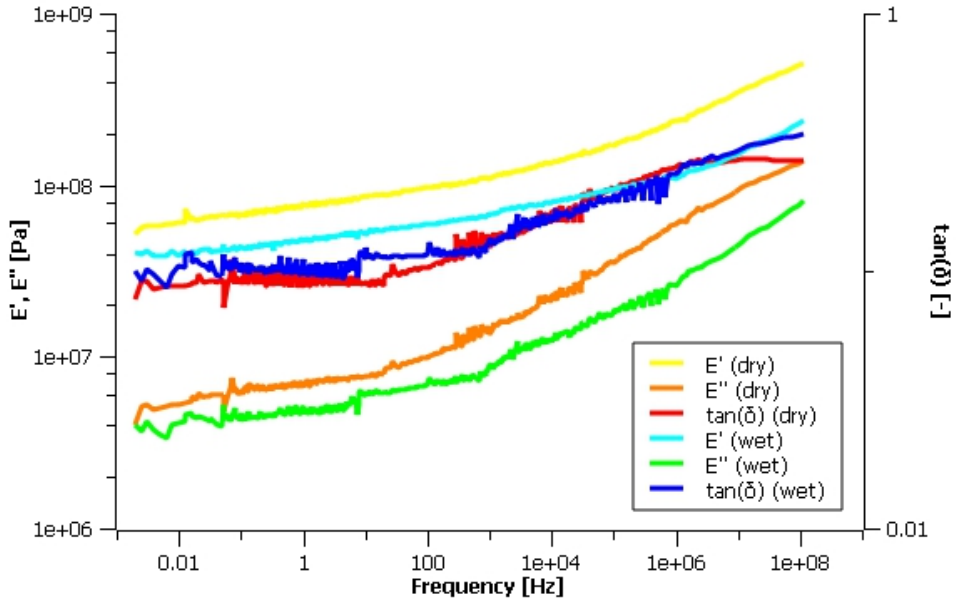

Figure 3.12: Master curve of the Time-Temperature Superposition (TTS) analysis for dried and saturated samples. Reference temperature: $40°C$.

were controlled to evaluate the effect on the incubation times of the impact frequency and the existence of dry intervals while testing, the two main Research Questions of this work. Regarding the water cushion, the air supply was active during every test from now on. This was the final choice as the coating in a real wind blade is subjected to high velocities and the water cushion is not expected to hold on the surface: the situation without the cushion is more representative of the real-life case [23]. For the humidity and temperature effects, two

filters were set to discard outliers when measuring incubation times. First, measurements that were performed outside the range of water temperatures (33-36 °C) were not considered. In this temperature range, properties are not expected to change according to DMA results (see Figure 3.10). Results were regarded when humidity was set higher than 95% RH. A second statistical filter was set to further limit the existence of outliers.

3.2 Impact frequencies

The incubation times were determined for different impact frequencies and velocities. Three frequencies (2.5, 27.7 and 42.6 Hz) and five velocities (130, 140, 150, 160 and 170 m/s) were examined.

3.2.1 Wöhler curves and Springer's models

Figures 3.13 show the Wöhler v_i-N curves for the given velocities and frequencies. A confidence interval of 95% has been incorporated into the plot. The number of impacts until incubation time has been plotted as the independent variable to make it more analogous to the fatigue curve. Table 3.6 presents the slope for the Wöhler curves for each impact frequency. The slopes have been obtained using the least-squares method. For the lowest of the velocities (130 m/s), just one experimental point was measured for each frequency. Those results were not used to estimate the Wöhler slope. For the lowest frequency (2.5 Hz), no damage was detected after 24 hours for 130 m/s.

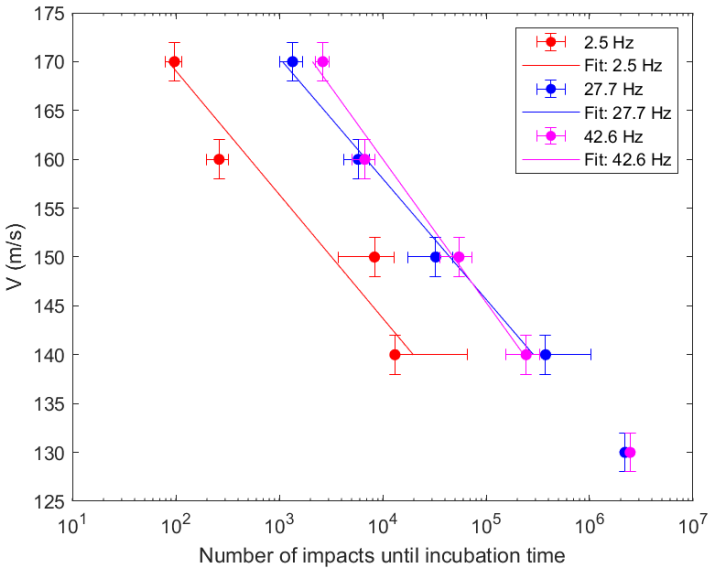

Figure 3.13: Wöhler curves in logarithmic scale for the three impact frequencies. A confidence interval of 95% has been added to the plots. Note: for the impact velocity of 130 m/s there are not confidence intervals, as just one measurement was taken. These points were not considered for the least squared method.

f_i (Hz)	2.5	27.7	42.6
m (-)	28.09	28.85	24.26

Table 3.6: Wöhler slopes for each impact frequency.

Figure 3.13 shows that the number of impacts until incubation decreases when increasing velocity with a power law. This trend is expected from a Wöhler curve. It can also be seen that the number of impacts until incubation decrease for lower impact frequencies. The Wöhler slopes are similar for every impact frequency, as all of them range from 24 to 29. Figure 3.14 plots the number of impacts until incubation time as a function of impact velocity for different impact velocities.

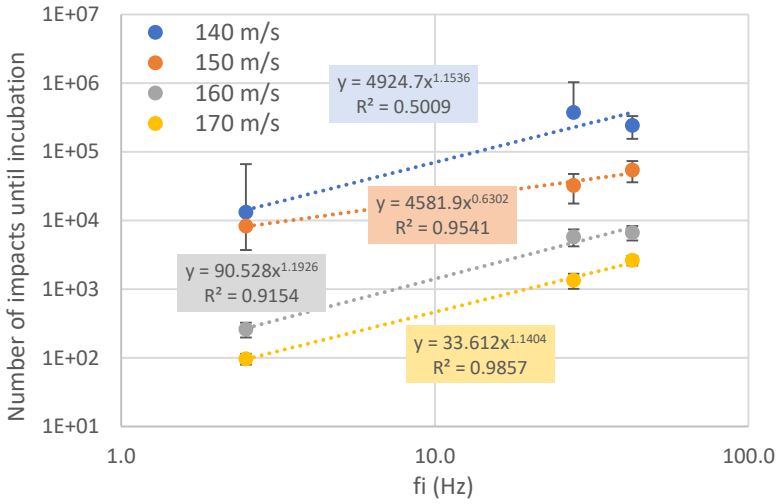

Figure 3.14: Number of impacts until incubation time as a function of impact frequency. A power law represents the best fit for the data points.

A power law was fitted that correlates very well with the data, especially for the experimental points tested at higher velocity (160 and 170 m/s). Note that more points were available for these velocities than for lower impact velocities (see Table 2.7).

The results were plotted in both Springer's models: the homogeneous and coated model. The assumptions of the Springer model were checked (see section 2.2.2). The hypothesis that accounted for a positive number of impacts were successful. The assumption for the homogeneous Springer's model that considers the thickness of the coating is large enough to consider it as a homogeneous material, however, was unsuccessful. The next formula shows how the inequality was not met.

$$h_c = 0.3mm$$

$$2d_d\frac{C_C}{C_L} = 2 \cdot 2\frac{1900}{1480} = 5.2mm$$

$$0.3 \not> 5.2$$

This means that the PU coating will go through stress reflections, while the model will not account for them. These reflections are detrimental to rain erosion performance, so the incubation times yielded by Springer's homogeneous model are expected to be lower than the actual values that were obtained in the experiments.

The other Springer's model is the model for coated samples. This model is based on the hypothesis that the thickness of the substrate is large enough to ignore stress reflections in this material (in this case, GFRP). This hypothesis is again not met for the tested coated samples:

$$h_S = 2.5mm$$
$$2d_d\frac{C_S}{C_L} = 2 \cdot 2\frac{1900}{2273} = 6.2mm$$
$$2.5 \not> 6.2$$

This would mean, again, that the model assumes that there are no reflections in the substrate, but in reality, these may exist. A minimum thickness of the substrate of 6.2 mm is needed for these reflections not to be present. Current Springer's model does not consider reflections in the substrate, so higher values of incubation times are expected to be obtained with the model. However, as the real and the assumed thickness have the same order of magnitude (2.5 vs 6.2 mm), the model may be close enough to reality. This situation, however, has to be kept in mind.

Figure 3.15 shows the representation of both Springer's model and the experimental data from this work. The original experimental data that was used to construct the model has also been added to the plots [34] [35].

The data points are quite aligned with both Springer's models. The same pattern that for the Wöhler curves emerges: for lower impact frequencies, the number of impacts until incubation is lower. For the homogeneous Springer's model, it seems that the impacts with high frequencies are better aligned with the model. For the coated Springer's model, however, it seems that low frequency impacts fit better into the model.

The confidence intervals for the Wöhler curve were added to the coated Springer plot. They were added to this model as it is the one expected to model more accurately the reality. The error in the parameters related to the strength and impact pressure ($\frac{S_e}{\sigma_0}$) was checked. From the parameters that were introduced in the model, the one that influenced it more was the velocity of sound in the substrate GFRP (C_S) (parameter present in Table 2.2. Figure 3.16 shows Springer's coated model with the error added to the experimental points.

When these errors are considered, the points may be considered to fit the data well. To know the fit better, it is compulsory to know a more accurate value of the speed of sound in the substrate. It has to be noted that, when varying C_S, the points undergo a shift towards the right or left (if C_S is lesser or a larger value, respectively), but every point would be moved in a similar way. Springer's model is a power law with exponent 5.7. Considering this speed of sound in the substrate, C_S, and for the current study, the slope of the power laws are 28.0 (2.5 Hz), 28.3 (27.7 Hz) and 25.8 (42.6 Hz). The cause that provokes this difference in the power law is not clear. It could be due to the viscoelasticity of the materials, but Springer data also accounted for PU coatings [32]. However, even with such a shift, experimental points seem to align pretty well with the model.

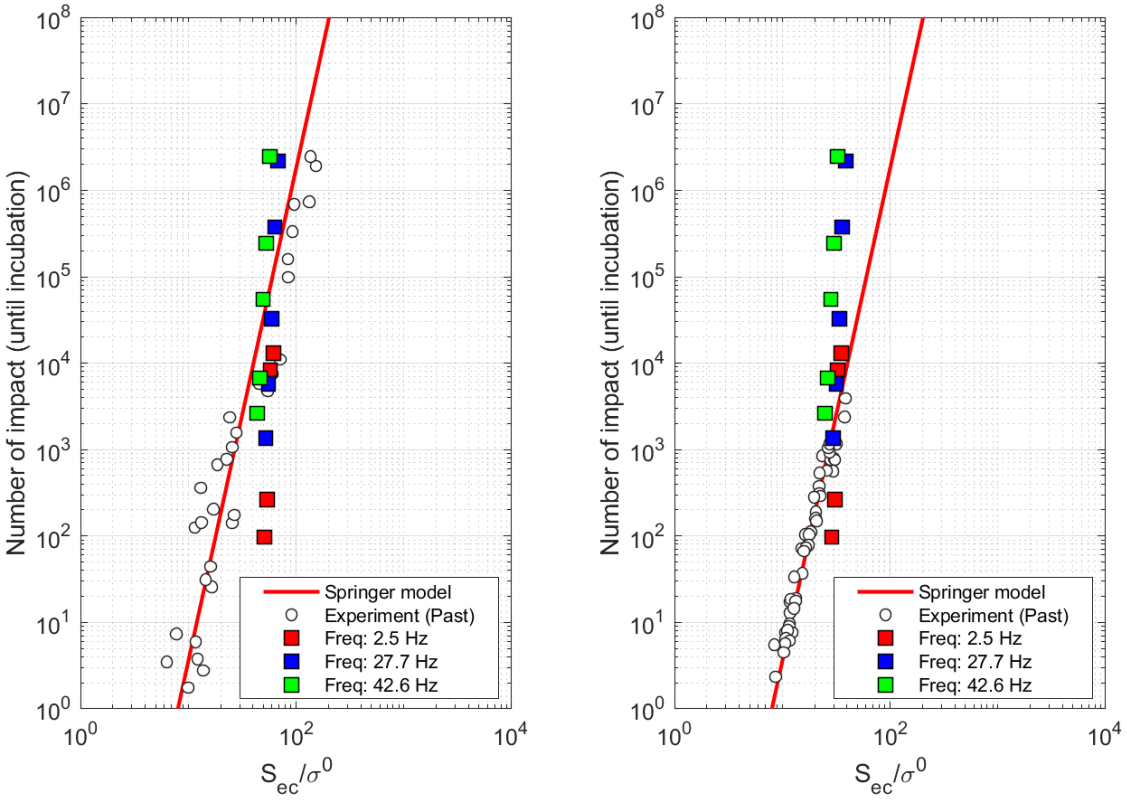

Figure 3.15: Experimental data plotted along both Springer's model: homogeneous Springer's model (a), and coated Springer's model (b)

3.2.2 Effect of raindrop length

The working principle of the PJET has been presented in past section 2.1.2. A rotating disk with holes chops the water slug that comes from the nozzle forming different droplets (see Figure 2.3). When varying the rotating frequency of the disk, the droplet impact frequency and its length vary. This is due to the working principle of the PJET: the disk rotates more slowly, thus, the section of the disk with the hole will be more effective time in front of the nozzle. This increased time results in longer droplets for low frequency impacts in the PJET. High speed footage of the moment of the impact are shown in next figures, for 10 m/s (Figure 3.17) and for 160 m/s (figure 3.18). Droplet length is also affected by the impact velocity. When the hole of the rotating disk is in front of the nozzle, a higher impact velocity will mean that more mass of water will be expelled at the same time, resulting in a longer droplet. This effect can also be observed in the high-speed footage.

Figures 3.17 and 3.18 show the change in droplet length when varying impact frequency and velocity. For low velocities, the droplet can be estimated using the footage. This estimation is more challenging for higher impact velocities, due to the mist created in the cabinet. Table 3.7 summarizes the estimation for the droplet lengths that were obtained with the high-speed footage. It is remarkable how for high velocities, the droplet is expected to have a higher length than the distance between the nozzle and the PU sample itself (5 cm). This high

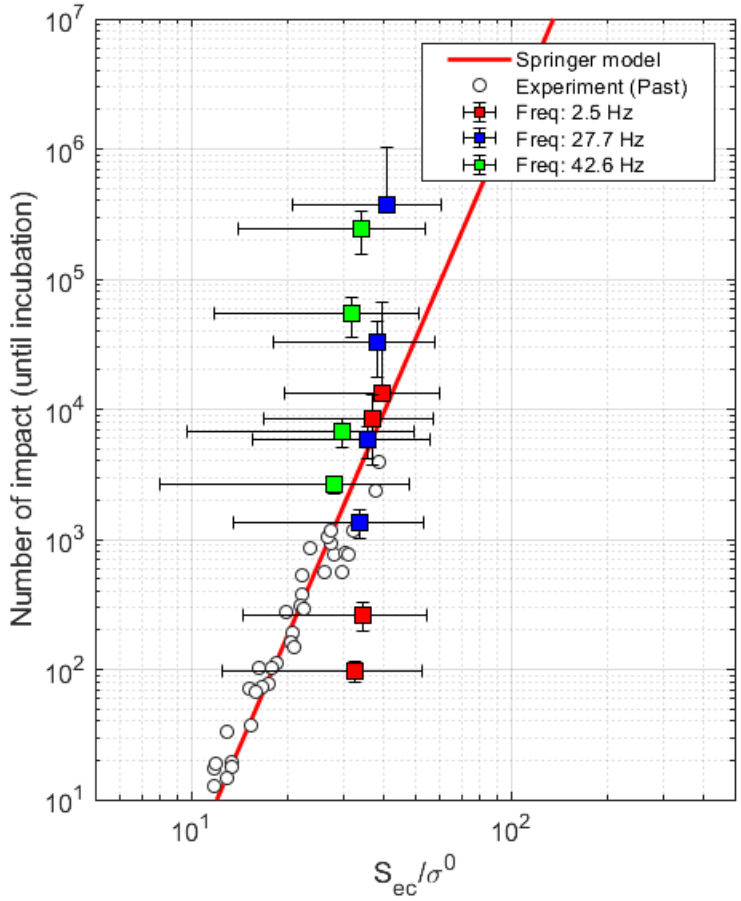

Figure 3.16: Experimental points plotted in Springer's coated model with the errors in measured incubation times (n_i) and speed of sound in the GFRP (C_S).

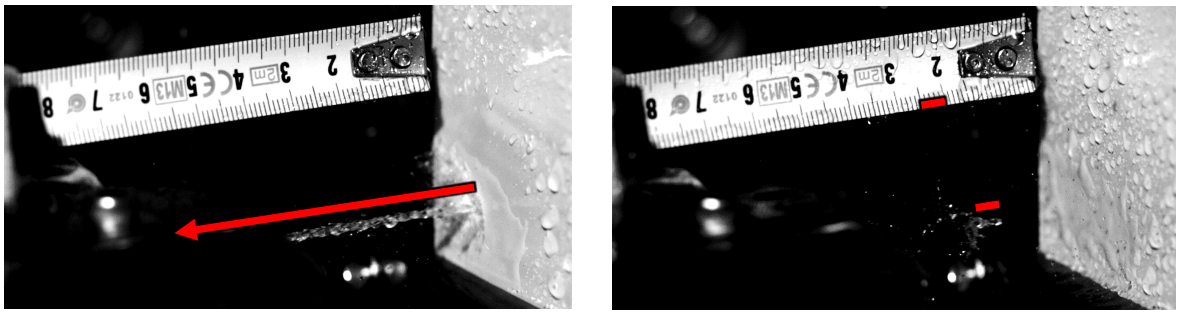

(a) (b)

Figure 3.17: Water droplet impact for 2.5 Hz (a) and 42.6 Hz (b) for an impact velocity of 10 m/s. Lengths of the droplets are marked in the images. For 2.5 Hz, the droplet length is longer than the distance between nozzle and coating (5 cm).

length is due to the large time of exposure that allows the formation of the droplet. This is, the time at which the hole of the rotating disk is in front of the water jet nozzle.

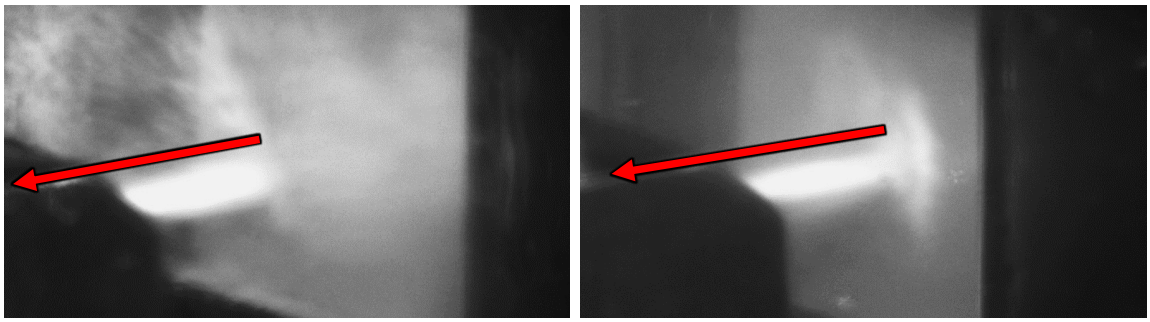

Figure 3.18: Water droplet impact for 2.5 Hz (a) and 42.6 Hz (b) for an impact velocity of 160 m/s. In both cases, the droplet length is longer than the distance between nozzle and coating (5 cm).

v_i, f_i	2.5 Hz	47.7 Hz
10 m/s	10 cm	0.5 cm
160 m/s	200 cm	10 cm

Table 3.7: Droplet length according to the high speed footage.

The effect of impact frequency on droplet length had already been investigated. Jonnson [10] examined the variation in droplet length in a similar PJET for different velocities (via pump pressure) and for different rotating frequencies of the disk. It was also concluded that the higher the impact velocity and the lower the impact frequency, the larger the length of the droplet produced by the jet.

The droplet length has been theoretically evaluated. The theoretical length was calculated by determining the time needed for the hole in the disk to displace itself through the jet expelled by the nozzle depending on its rotating frequency. This approach is similar to the one used by Jonnson when assessing the theoretical length of PJET droplets [10]. Some geometrical assumptions were set to carry on the results. The whole theoretical process of these calculations is included in Annex I. The final equation that defines the theoretical droplet length depending on the frequency was found to have the following expression (for this specific PJET). Table 3.8 shows the droplet length that was theoretically obtained for the cases observed with the high-speed footage.

$$l_{drop} = 2.73 \cdot 10^{-4} \frac{1}{f_i} \cdot v_i(cm) \tag{3.1}$$

v_i, f_i	2.5 Hz	47.7 Hz
10 m/s	10.9 cm	0.6 cm
160 m/s	174.4 cm	9.2 cm

Table 3.8: Theoretical droplet length. Increasing the impact frequency makes the single droplet shorter.

The correlation between the two lengths, the ones measured via high-speed footage and the ones obtained theoretically, is high. This high correlation validates this method of calculating

the droplet length. According to the theoretical length equation, droplet length is expected to vary inversely proportional to the impact frequency, via a power law with slope -1. That fact provokes such a high droplet length for low frequencies (up to 170 cm).

The theoretical droplet length was calculated for the whole range of frequencies of the PJET, from 2.3 to 47.4 Hz. The results were plotted in Figure 3.19, as well as with the measured values of length via the high-speed camera. To observe that the trends were comparable to the ones that Jonnson observed in their PJET, the experimental points measured in their work have been also plotted. The trends confirm that for lower frequencies, length rises. For the impact velocity chosen (10 m/s), droplet length is increased by a factor of 20 when changing the frequency from 2.5 Hz to 47.7 Hz. The trend for the theoretical length is comparable to the one observed for Jonnson's results: a power law with a slope of -0.942 was reported, close to -1. Jonnson measured more impact frequencies for more impact velocities, but they are not comparable to the present work as here just a velocity of 160 m/s was used [10].

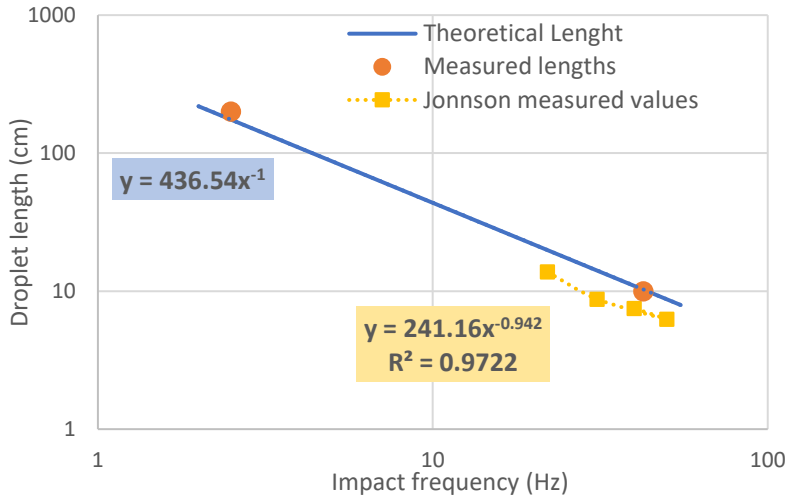

Figure 3.19: Droplet length as a function of impact frequency for the DUCOM jet. The theoretical length, as the two values that were measured via high speed footage have been included. Jonnson's results, which evaluated droplet length for a similar jet have been included and fitted [10].

A longer droplet means that the droplet is expected to carry more energy for the same impact velocity. Based on the kinetic energy equation, this relationship between energy and length is expected to be linear. The parameters d_d and l_d refer to the diameter and length of a single droplet. As the energy rises linearly with the mass of the droplet, it is expected to rise linearly also with droplet length. The equation of the theoretical kinetic energy can be established:

$$E_d = \frac{1}{2} \cdot \frac{\pi}{4} d_d^2 \cdot l_d \cdot \rho \cdot v_i^2 \tag{3.2}$$

Table 3.9 shows the theoretical impact energy of each of the droplets analyzed with high-speed footage. The droplet diameter (d_d) has been set to 2 mm.

The other secondary effect of increasing the droplet length is the raise of lateral jetting effects. The longer the droplet, the longer time that lateral jetting effects are present. The more

v_i, f_i	2.5 Hz	47.7 Hz
10 m/s	0.017 J	0.001 J
160 m/s	69.920 J	3.688 J

Table 3.9: Theoretical droplet energy for each droplet.

prolonged lateral jetting may be tearing away more quickly imperfections in the material, and thus, reducing the incubation time.

To check the dependency of the number of impacts until incubation and impact energy, the Wöhler $v_i - n_i$ curves (see Figure 3.13) were again plotted in different ways to account for these factors.

3.2.3 Number of impacts vs. testing time

Until now, incubation time has been presented as number of impacts. The advantage of this method of presentation is that the results can be correlated easily with the Springer model, which considers the number of impacts per site [32]. However, there are other ways of measuring the incubation time. The test standard ASTM G73 [54] recommends plotting the cumulative coating mass loss versus the exposure time, or testing time. This option of representing the results is the most common way in literature [37]. This way of representing the results does not account for other factors, such as the amount of water that hits the material. Other authors have reported the impacting water: Mahdipoor et al. [55] reported the mass loss of the coating versus the volume of impacting water; Seleznev et al. [56] used the mass of water. Again, these methods have drawbacks as they do not reflect some testing parameters, such as the impact frequency that is been addressed in the present research project.

The results for the Wöhler v_i-N curve (Figure 3.13) have been plotted again for different x-axes. Figures 3.20 show the number of impacts until incubation time with velocity, but now also the cumulative volume of impacting water; the global testing time ($t_i(s)$) and the cumulative impact energy until incubation.

When considering the number of impacts until incubation time (Figure 3.20, a), there is a clear shift in the Wöhler plots depending on impact frequency: for lower frequencies, the Wöhler curves are shifted to the left. This shift is not present in the other plots that do not present the number of impacts, like the testing time (b), cumulative impacting water volume (c) or cumulative impacting kinetic energy (d). For these three ways of measure the incubation times, all frequencies same to be quite correlated. These three ways of measure the incubation period are interconnected and account for the fact that the droplet is longer for low frequencies. Again, change in the Wöhler slope cannot be observed for any of the curves.

3.2.4 Damage evaluation

The tested samples were inspected with a 3D microscope to look for different damage features. Attention was paid to the predominant damage modes (pitting, adhesive problems or cracks)

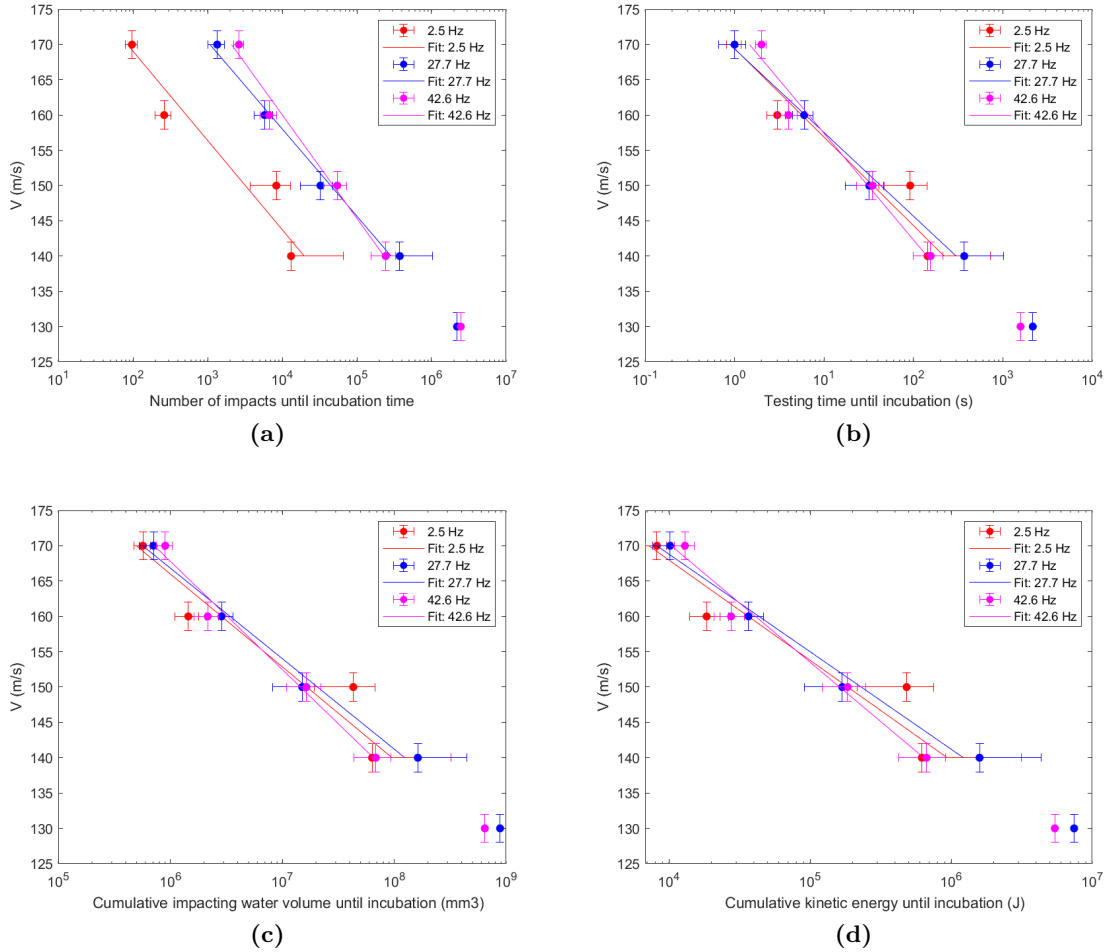

Figure 3.20: Four different ways of plotting the results of incubation times versus impact velocity: number of impacts (a), global testing time (that the PJET was active) (b), cumulative impacting volume of water (c), and cumulative kinetic energy. All plots are referred to the end of the incubation period.

and plastic area size. Early forms of damages were compared to investigate differences between various parameters, such as impact velocity and impact frequency.

The behaviour of the sample during testing and the damage evolution was generally the same: after some time, a small plastic zone appears at the hitting point, very localized. This plastic zone grows until it has a certain size. The plastic zone remains stable for some time, and at some point, the coating undergoes damage that can be visually inspected. This first damage is considered the end of the incubation period. Pictures of the sample prior to any damage and after testing can be seen in Figure 3.21. The plastic zone can be appreciated in the heightmap.

The sizes of the plastically deformed areas were measured and compared for different impact velocities and frequencies. In the height maps, two different radiuses are observed: an internal and an external radius. This is due to the fact that the plastic zone has an annular form. When increasing the velocity, the plastically deformed ring-shaped area tends to increase. Figure

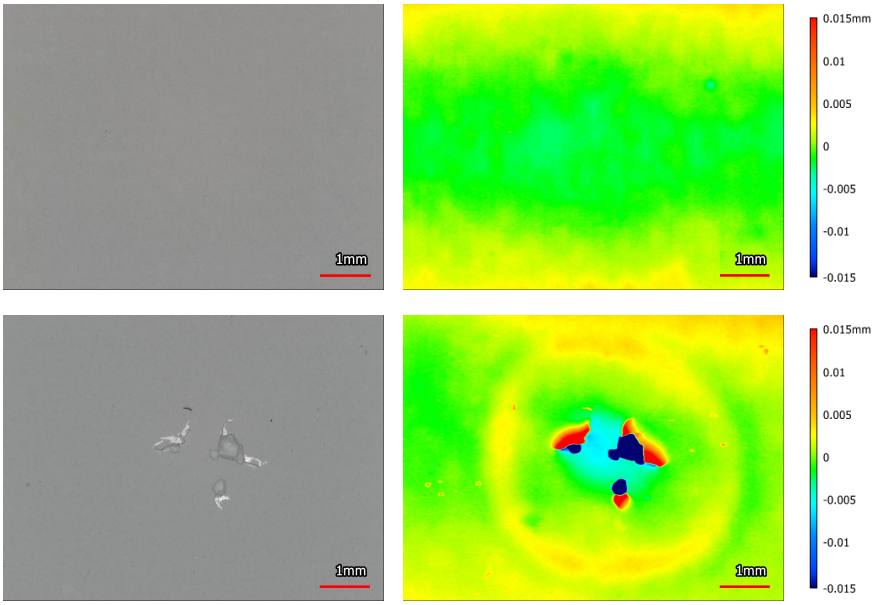

Figure 3.21: Surface of the polyurethane coating before and after carrying out erosion tests. The tested sample was tested at 160 m/s and 47.7 Hz.

3.22 shows this increasing trend. The size of the deformed area does not change significantly when changing impact frequency, given its standard deviation is taken into account. The measurements of these radiuses depending on impact velocity and impact frequency are shown in Figure 3.23. The damages that occurred at 130 m/s were not considered as there was just a limited number of data points not to be representative.

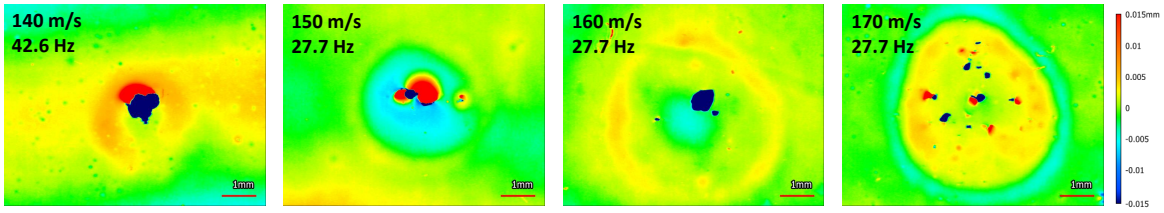

Figure 3.22: Different damages for increasing values of impact velocity.

The microscope analysis of the samples shows different damage mechanisms and features. Those are mainly pitting, cracks and debonding mechanisms. For the great majority of damage points, there is one of the mechanisms that is more dominant than the others. It has been tried to correlate the various damage mechanisms with impact velocity, impact frequencies or the time that the sample was in the cabinet (to know if they were related to humidity). No correlation was found between all those: for different velocities and impact frequencies, the coating show similar damages. This lack of correlation may indicate that the difference in damage features is due to the sample itself and the manufacturing defects that the batches could have. Figure 3.24 shows some examples of these damages which have been chosen as representative of the rest of the samples.

Specific features were found for some damage spots that were tested at low frequency (2.7 Hz)

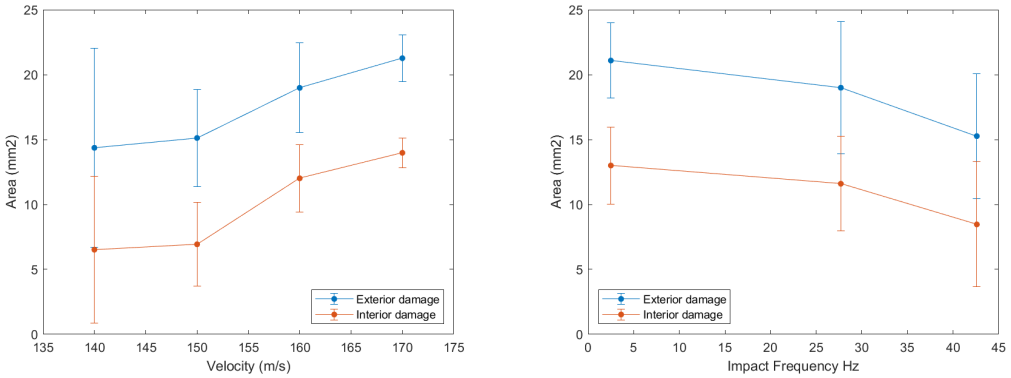

(a) (b)

Figure 3.23: Evolution in the exterior and interior plastic radius for different impact velocities and frequencies.

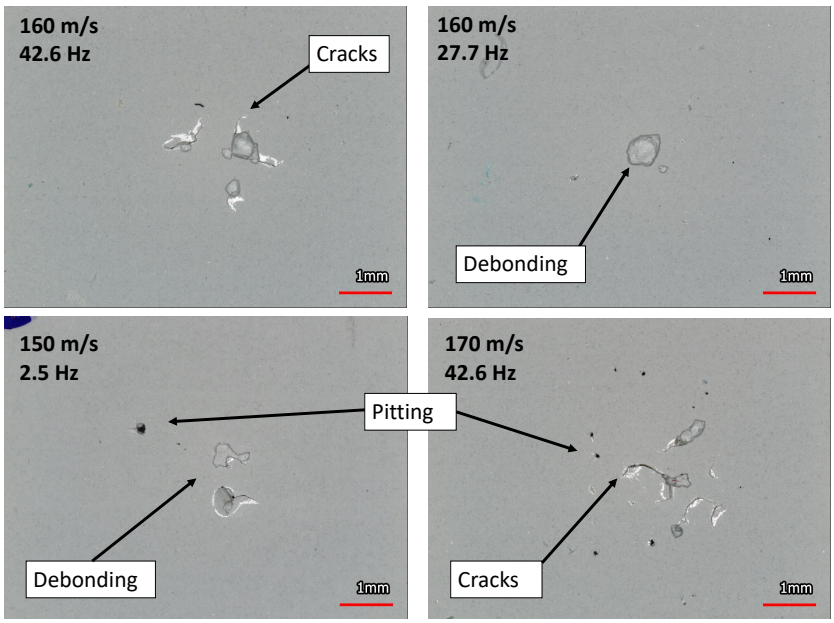

Figure 3.24: Different damage features observed across the samples.

and for different velocities. Those damages consist of characteristic cracks around the impact main damage and were not found for higher frequencies. Pictures showing this damage feature are shown in Figure 3.25. However, these damage features were not always observed: there were tests at low impact frequencies which did not show these cracks at all. Height maps of these damages reveal that they are small areas of coating elevated above the baseline.

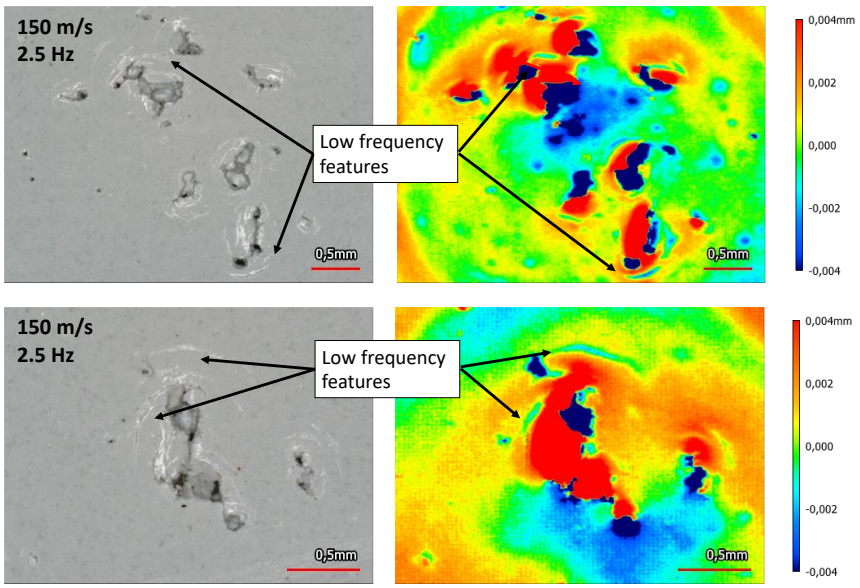

Figure 3.25: Cracks characteristic for low frequency impacts found in the damages. Presented data points were tested at 150 m/s. Darker areas represent valleys below the baseline, while red areas represent areas above it (up to 0.004 mm).

3.3 Dry intervals

This section addresses the results of the dry intervals tests. The ratio r represents how much the time until incubation rises when stops are performed compared to the case where there are no stops. As the impact velocity and impact frequency were fixed, there is a justification to focus just on this parameter instead of looking at the number of impacts until incubation (n_i) or global testing time until incubation (t_i).

Figure 3.26 shows the measured r values for the different combinations of dry interval parameters: λ, α and β. Note that the point $r = 1$ has also been plotted in the figures. This point represents the value at which no dry intervals were performed. Table 3.10 shows the values of ratios for every combination of parameters. There are some results of r that do not have deviation. This is due to the fact that just one test could be carried out for this set of parameters.

For all cases in which dry intervals were tested, the mean of the ratio r was greater than one. This means that, on average, the time until damage appeared in the sample increased when performing dry intervals.

A factorial analysis was carried out to know how the dry intervals parameters (λ, α, β) may influence the ratio r and their significance in the results. The main effects were studied and their statistical significance through Pareto plots in Figure 3.27.

The Pareto chart 3.27 shows that two parameters may be statistically significant: λ, which represents the duration of the dry interval, and α, which represent the time at the stop is set. These two values surpass the reference line, which indicates that the effects are significant. The number of stops (β) appears not to be statistically significant. According to the Pareto chart, the value λ has the largest effect on the means of the measured ratios r. The main

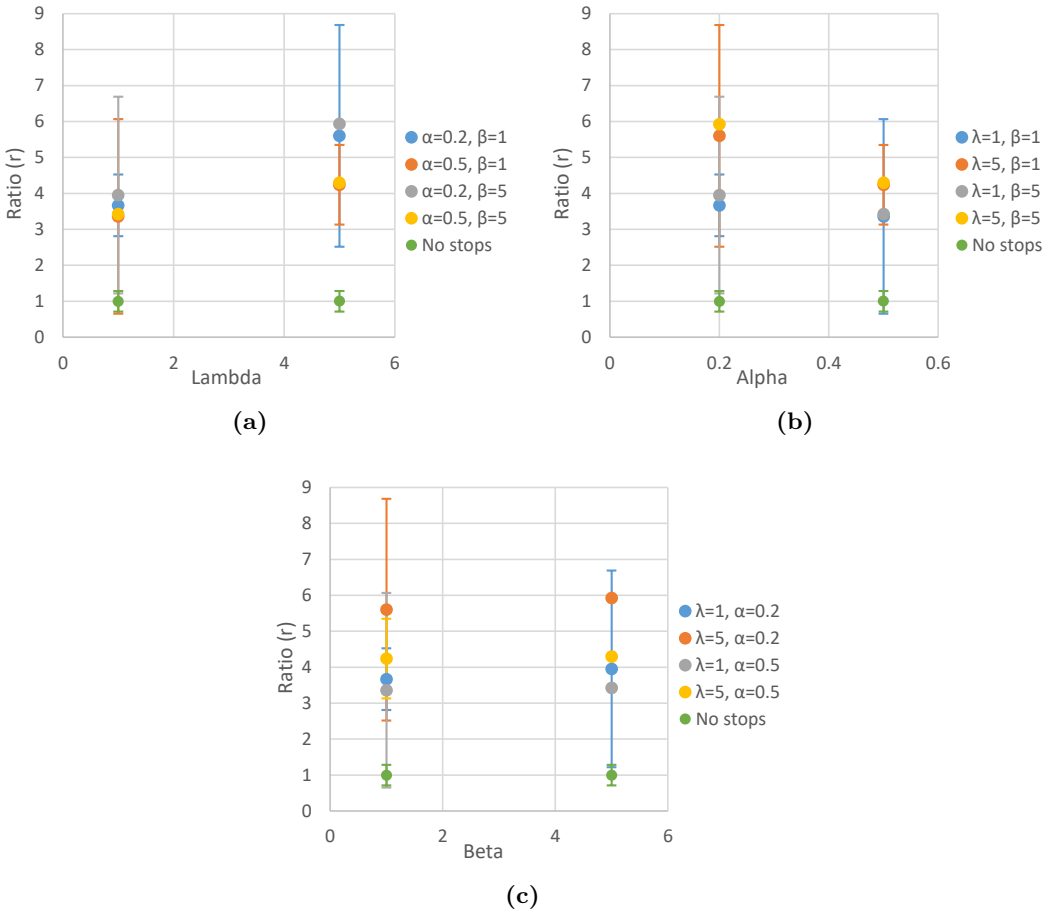

Figure 3.26: Ratios obtained during the dry interval experiments. Three scatter plots are set for each parameter: λ (dry interval duration), α (moment then the interval starts), and β (number of stops).

λ	α	β	r
0	0	0	1.00 ± 0.29
1	0.2	1	3.67 ± 0.86
1	0.2	5	3.95 ± 2.73
1	0.5	1	3.36 ± 2.71
1	0.5	5	3.43
5	0.2	1	5.60 ± 3.08
5	0.2	5	5.93
5	0.5	1	4.24 ± 1.11
5	0.5	5	4.30

Table 3.10: Values of r obtained during the interval tests for every combination of parameters.

effects plot show that when lambda is increased in the range (1-5), the ratio r increases from about 3.5 to 5. For alpha, when alpha increases in its range (0.2-0.5), the ratio decreases from

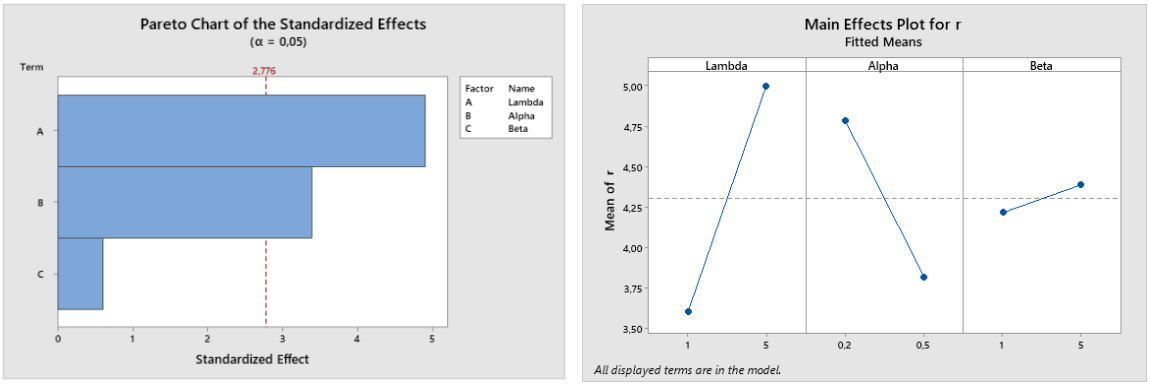

(a) (b)

Figure 3.27: Factorial study of the ratios for the three stops parameters: λ, α and β. a): Pareto study for (confidence interval of 0.05). b): Factorial analysis for the parameters.

about 4.75 to 3.75. When varying beta, the main effects plot of its effect in the ratio is not much, and its line remains almost horizontal.

The p-values of each factor were compared to know if the parameters are statistically significant. Table 3.11 show the p-values for each parameter. Coefficients are also shown. These coefficients represent the change in the mean response for a one-unit increase in the factor, while the rest of the terms are constant [50]. The p-values for the parameters λ and α appear again as significant.

Parameter	P-Values	Coeff.
λ	0,008	-0,700
α	0,027	0,484
β	0,578	-0,086

Table 3.11: Table showing the p-values and coefficients for the dry interval analysis. Significance level: 0.05.

It was investigated if the general full factorial model fits the data by examining the key parameters S and R_{sq}. S represents how far the measured values are from the fitted values and it is measured in the same units that the response (in this case, the units of r are dimensionless). A lower value of S suggests that the model may be correct. R-squared (R_{sq}) is a statistical measure that represents the proportion of the variance in the response that can be explained by the factors of the regression model. It is measured as a percentage from 0 to 100 %. The higher the R_{sq} value, the better the model fits the data. For the present study of the ratios r, values of $S = 0.40$ and $R_{sq} = 89.99\%$ were obtained.

The residual plots for the factorial design were evaluated. The residuals versus fits are expected to be randomly distributed and to have a constant variance with no recognizable patterns. For the present work, it was observed in the residuals versus fits plot that uneven spreading of the residuals may be taking place. This may be true, as it is true that the experiments had to be stopped while testing and every experimental point could not have a similar deviation.

Chapter 4

Discussion

4.1 Erosion test parameters

4.1.1 Water cushion

The effect of the water cushion was examined. The high-speed footage provided evidence for the existence of this water cushion for low velocities (10 m/s). However, its existence cannot be assured for high velocities, as the mist prevents any footage. When impact velocity is increased, so is the lateral jetting velocity. For impacts velocities of 160 m/s, lateral jetting may go up to 2000 m/s [27] [7]. Therefore, it is expected that water cushion effects are less severe for higher velocities: its removal is granted for higher velocities. The thickness of the water cushion could not be evaluated with this setup.

It was hypothesized that the water cushion would affect more heavily higher frequencies. The change in the lognormal parameters observed in the lognormal fits (see Figure 3.3) were noted in Table 3.2. Every lognormal parameter (mean, median and mode) increases for higher frequencies (42.6 Hz) when the air supply is active, which indicates that there is a water cushion effect that is effectively raising incubation times. Table 3.2 shows a slight decrease in the lognormal parameters for lower frequencies (2.5 Hz and 27.7 Hz). This decrease has been linked to the change of shape of the lognormal function. This change of shape can be observed in Figure 3.3. The lognormal fits for lower frequencies (2.5 Hz and 27.7 Hz) have their peaks quite close in both cases: with the air supply active and inactive. For high frequencies (42.6 Hz), the peak is shifted. This effect is clear when looking at the change in the mode of the curves (see below Table 4.1). Figure 3.3 also shows that the shape of the fit functions for lower frequencies change, which is likely to be causing the changes in mean and median that are shown in Table 3.2. This change in the shape of the lognormal function could be due to the higher variability of the results when the air supply was active. It could also happen that the air supply is affecting the water droplet impact. However, this hypothesis could not be verified.

The water cushion effect has been previously investigated by other researchers, but there has been debate in the literature about its consequences. Brunton et al. [57] suggested that the

f_i	Mode
2.5 Hz	-11.4
27.7 Hz	-2.4
42.6 Hz	+79.0

Table 4.1: Effects (%) in the modes of the lognormal fits when there is not water cushion effect (air supply active). The reference is set for the case when water cushion effect may exist (air supply inactive).

water cushion may reduce damage: the liquid film would deform upon impact and would reduce impact pressure. It was also hypothesized that the divergence of stress waves through the film may reduce the damage to the coating. The thickness of the water cushion is expected to be important, but critical film thickness was not mentioned [23]. Some researchers, as Shi et al. [22] concluded, while testing aluminium samples with erosion jets, that in some cases, liquid of the water cushion can get trapped in cracks, enhancing more damage. Zhang et al. [23] investigated the water cushion effect and concluded that it is recommended to use an air blower to replicate better conditions at the WTB, after finding that water cushion may accelerate erosion evolution with a jet-slug experimental setup.

Based on the results of this work, it can be concluded that a water cushion effect has been observed in the present work, but just for higher impact frequencies. The mode of incubation times was increased by a factor of +79% for higher impact frequencies, while there was a small change for lower impact frequencies (−11% and −2%) that could be explained due to the deviation of the results and change in the lognormal shape. These results are in line with Brunton's conclusions [57]: that the water cushion is expected to dampen the energy of the next impact, decreasing the water hammer pressure. With the air supply, this effect is cancelled out.

4.1.2 Temperature and humidity

Figure 3.9 shows the decreasing trend of incubation times that are measured throughout the day, converging to a certain value over time. This effect has been linked to the temperature of the water and the sample and the humidity in the cabinet. The decrease has also been related to the saturation of the sample, as samples that went saturated at the CTS converged faster.

During the experiments, the measurement was considered successful when the water tank had a temperature between $33 - 36°C$, when the temperature got stable. This stabilized temperature appears to be higher than the water temperature observed in other research projects which used PJET's: 22°C [58] or $20 - 25°C$ [59]. One of the limitations of the experimental setup is that the temperature of the water cannot be effectively controlled, as it relies on its stabilization by the cooler. Figure 3.6 shows the trend of incubation times with water temperature: the higher temperature, the lower incubation times, especially for higher frequencies. However, the high clustering of the results may challenge the hypothesis of the direct effect of water temperature on incubation times. These plots were obtained at the same time that the water cushion effect was being investigated; thus, the effect of water temperature was not the main focus of this set of tests. The high correlation obtained is likely

due to few points with a very high and very low temperature that affect much the results. It is remarkable how the fit for low frequencies (2.7 Hz) did not show any correlation, while the fit for the two other frequencies did. This behaviour could be explained by the fact that for high frequencies, much more mist and tiny droplets appear in the cabinet than for lower frequencies. This extra humid environment could saturate the coated sample faster than for lower impact frequencies. The relative humidity according to the sensor was the same for all impact frequencies (95% RH), but it is plausible that the sensor gets saturated for very high humidity.

It was hypothesized that the sample was absorbing water and affecting the results. The water uptake obtained from coating PU samples without substrate in the CTS (see Figure 3.7) shows that samples tend to be saturated relatively quickly, after around one hour in a warm and humid environment. In this time, the coating has had time to be soaked and their impact properties could have been modified. This soaking time makes sense with the observations at the PJET: as 3.9 shows, the first measurements in the PJET (for a dry sample) can take up to more than an hour. This time is enough for the sample to be saturated. The shape of the water uptake curve (Figure 3.7) is in line with other uptake curves observed in literature for the absorption of PU [60]. The oscillations in the uptake curve, when measured from 1 to 6 hours, may be explained due to the time spent to take the samples to the balance to be weighted. It has to be acknowledged that the law for uptake for the coating itself (see Figure 2.10) is different to the water uptake law in the composite and the substrate. However, it should give a reference value at which the coating gets saturated.

Figure 3.9 also shows how, even though the coated samples were taken straight from the CTS into the PJET, the incubation times are still higher for the first measurements. This fact could point out to a high reversibility of the mechanical properties when the environment is not humid anymore. Some time (around 15 minutes) is needed to attach the sample to the sample holder and start the testing. This time at room temperature could be enough for the properties of the sample to go back to the original (not soaked) state. Another factor that supports the hypothesis of the reversibility process is that after pauses were performed while testing (that lasted about one hour), times were again observed to increase as at the beginning of the day. It was hypothesized that, during this time, the coating could have time to recover itself from the humid environment.

The effect of water absorption and its consequences on the mechanical properties of polymers have been studied in different research projects. Boubakri et al. [61] studied the effect of moisture absorption in tensile test properties of thermoplastic polyurethanes. A decrease in bulk material properties was found for samples that had been immersed for 6 months at 70 $^{\circ}C$. Their latter work [62] found out that the decrease in mechanical properties is dependent on water temperature. After these humidity treatments, lower concentrations of hydrogen bonds were found. A "plasticization" effect in polymers was observed that caused a decrease of its Tg, shifting its elastomeric range and bringing down the storage modulus [62]. Similar effects have been found in the present project in the TTS plots (see Figure 3.12). The drop in properties was also linked to some small voids in the PU samples. Jana et al. [63] performed hygrothermal aging cycles to thermoplastic polyurethane samples and arrived at similar conclusions. The reversibility of this process was assessed by Boubakri [61], which dried for 2 days aged samples. Other researchers that studied specific polymers, shape memory polyurethane foams, concluded that the process was reversible when heat was applied to the soaked samples [64].

More research has been carried out on shape memory polyurethane foams, which also have a hard and a soft phase, as the PU coating that was tested in this work. Yu's research [60] found that water uptake in these foams raised until 8% and get saturated after 6 hours. When saturated, the Tg dropped, failure stresses and Young's modulus decreased and strain at failure increased. The water acted as a plasticizer: water molecules penetrate into the polymer chains, preventing them from moving freely. Yu's work concluded that these effects were also reversible after placing the sample at humidity levels of 40% for 24 hours. All the cited researchers carried out tensile tests not focused on high frequency problems (as Leading Edge Erosion is). The effects of moisture on mechanical properties for high frequency may be different.

There appears to be a general consensus on the effect of humidity in the drop of mechanical properties due to plasticization. The plasticizer effect of water may explain the change in incubation times over time and for dried and soaked samples (see Figure 3.9). As the sample gets more exposed to the humid ambient in the cabinet, the polymer absorbs water and their mechanical properties change, resulting in a lower incubation time. When the coating cannot absorb more water, the incubation time converges. Figure 3.9 shows still an initial peak in the measurements of saturated samples. This peak may be due to two causes. It has been hypothesised that the coating undergoes while testing is more extreme than it was thought. The CTS was set at the environmental conditions that were recorded in the cabinet via thermocouples (see the thermocouples in Figure 2.6) and humidity sensors: 38°C and 95 % RH). However, these thermocouples were installed at the back of the sample. Maybe droplet impacts are increasing the temperature locally in the PU coating much more than the value which was measured with the thermocouples. Literature shows that the drop in mechanical properties due to humidity are more prominent for higher temperatures [62]. This would explain why saturated samples that were treated in the CTS still needed some time for their incubation times to converge to a certain value. The initial peak in incubation times for wet samples could also be due to a very high reversibility of the saturation process: the wet sample had still to be set in the PJET. The placement in the PJET could take around 15 minutes and may be enough for the coated samples to recover their properties before the humidity treatment. This hypothesis of very high reversibility of the saturation process is in line with the findings of Yu and Yang [60] [64], which investigated shape memory polyurethanes. However, in their works, the polymers needed high temperatures or large times to recover.

DMA analyses were carried out to know the change of properties of bulk PU samples. The temperature scan (see Figure 3.10) showed that there is a drop in the storage modulus (E') and loss modulus (E") when increasing the temperature, both for dry and wet samples. The shift of $\tan(\delta)$ for wet samples indicates that there is a change in the T_g. The decrease in T_g can be linked to the phenomenon of plasticization, as said above. The TTS analysis (see Figure 3.12) concludes that E' and E" are reduced when the sample gets saturated. This change in properties is also linked to the plasticization process. So, it is likely that this process happens in the sample when tested.

Research literature has tried to connect the viscoelastic properties with rain erosion performance. O'Carroll et al. [17] found a correlation for the storage modulus of polymer LEE coatings: as the elastic modulus (measured at low frequencies) was reduced, incubation times increased. Arena [44] evaluated pure PU samples (not coated samples) using sand erosion, and found the following correlation: the higher the E' and E" obtained for higher frequencies

(via DMA), the larger the mass loss. The incubation time was not investigated in their work. These findings may indicate that lower values of E' and E" improve the rain erosion resistance. However, the findings of the present work may point out to another direction: as E' and E" drop (due to the temperature increase and the saturation of the sample), the incubation time of the sample decreases. Furthermore, the changes in the properties of the coating and its water uptake may be affecting the interphase between the PU coating and the substrate. This interphase is one of the most critical features of a PU LEE coating [5]. If this was the case, adhesive failures should have been found in the microscope for the damages related to saturated samples. This kind of feature was not observed in the microscope analysis: there were similar damages failures for all cases, dry and wet samples. However, the effect on the coating interphase cannot be ruled out.

In summary, the experimental results show that temperature and humidity are playing a role in the incubation times of the coated samples. DMA analyses reveal that both the storage and loss modulus decrease when temperature increases and the sample absorbs water. Similar environmental situations are known to lead to plasticization of PU, which may reduce the failure stress of the samples [60]. This reduction in properties may be causing the drop in the incubation times of the samples.

4.2 Impact frequencies

The first key research question of the present work was linked to the incubation times for different frequencies. Based on the viscoelastic properties, the rain erosion performance of the material was expected to increase, since they will have more time to recover themselves from the previous impacts. The two extreme frequencies used in the project, 2.5 and 42.6 Hz, had very different relaxation times between impacts: 0.4 s and 0.02 s, respectively. This difference was expected to make incubation times increase for lower frequencies.

This behaviour was not found in the results (see Figure 3.13: for lower impact frequencies, the incubation times were lower. The effect of the water cushion was discarded as it had already been investigated separately. The slopes of every Wöhler curve were very similar, which indicates that the number of impacts until incubation were affected in the same way by velocity regardless of the impact frequency. In the end, the Wöhler slope is related to the material itself, so it is logical that it remains constant [25]. A power law with a constant of +1.15 was able to describe the evolution of incubation times with impact frequency (see Figure 3.14).

The lower incubation times for lower impact frequencies could not be explained by the viscoelastic behaviour of the PU, but it could be explained by the change in the length of the droplet. Although droplet length may be the cause for the observed change in incubation times, that does not mean that there are not viscoelastic effects taking place, they just may be hindered by the effect of the droplet length. This could be possible, as viscoelastic effects were effectively found when dry intervals while testing were performed. Figure 3.19 shows the theoretical length as a function of the impact frequency. Incubation times were then found to have a power law of -1.15 when droplet length was considered, shown in Figure 4.1. The power law found was -1.15, logical, as the theoretical length that was used was inverse to the impact frequency. This value of -1.15 can be compared with values that link the erosion rate

with the diameter of the droplet size. Hattori et al. [65] found a 4.67th power of the mass loss rate with the droplet diameter when studying aluminium and steel samples in a jet. The influence of droplet length is smaller than the trends for droplet diameter. However, it was found to have an effect.

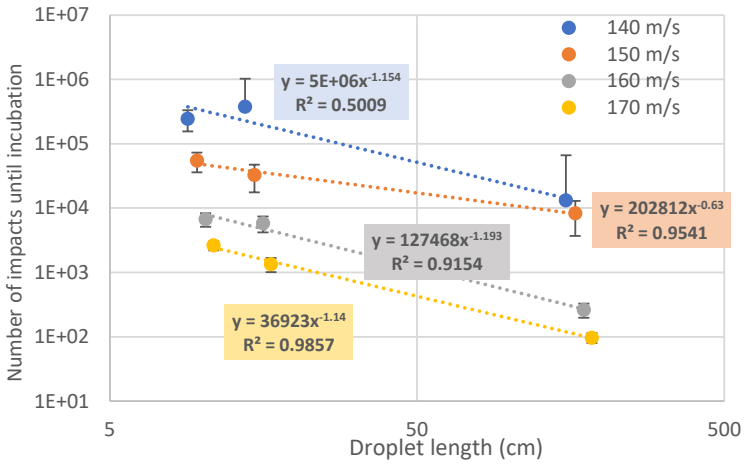

Figure 4.1: Number of impacts until incubation depending on the droplet length. Theoretical lengths (see Annex I) were considered.

A relationship with droplet length is suggested. The jet length has been considered to have an influence on rain erosion in the literature, but it has been normally neglected. According to Jonnson, this fact has been due to the fact that PJET approach relies on the impact and compression stresses [10], which makes the erosion processes comparable for different lengths. That could be true in the case of shorter droplets in the PJET when there is not much difference between the length (as in Figure 4.1 between 10 and 16 cm of length). This effect could be nullified when comparing different coatings in a single PJET setup or when varying parameters keeping the droplet length constant. But droplet length could be an issue when comparing results measured in the PJET with other facilities, such as whirling arms. Correlation between both setups has been proven very challenging [23]. The whirling arm facility is based on a totally different approach: the sample is impacted against a rainfall [37]. The droplet size for this rainfall is expected to be about 2 mm [17], which is considerably less than the 10 cm length obtained in the PJET. There are more differences between both facilities that difficult their correlation (for example, the fact that the PJET damage is far more localized [37]). But the difference in droplet length may be important. The effect of droplet length that has been observed makes for the argument that it should be considered as a testing parameter, especially when comparing different PJET facilities.

Increasing the droplet length has several direct effects on the impact. It prolongs the duration of the initial pressure and the effect of lateral jetting. It also enhances the kinetic energy of the impacting droplet, as it is more massive. Impact pressure has been found to increase with droplet diameter [38], so a similar effect may be happening when increasing its length. The fact that, when kinetic energy and impacting volume is considered in the Wöhler curve, the values for every impact frequency match (see Figure 3.20) shows the importance to know exactly the shape of the water droplet when comparing results from different testing events.

When the results were introduced into Springer's model (see Figure 3.15), some of the assumptions of the model were not met: the model does not account for stress reflections between the coating and substrate interphase (in the homogeneous model) and at the end of the substrate (in the coated model). These reflections are expected to reduce the rain erosion performance, so experimental points are expected to under-perform Springer's model predictions. However, experimental points in both models are for the most part aligned with the model. For the coated Springer's model (see Figure 3.15, b), low impact frequency points are shifted to the right, while high impact frequency points are shifted to the left of the model prediction. This is again due to the difference in length and energy of the droplet. Springer's model does not acknowledge the effect of energy per impact: the model does not grasp a difference between the 2.5 Hz and 42.6 Hz droplet, although they are essentially different: the P parameter (impact pressure) is the same regardless of the impact frequency. This fact explains why the points for all three frequencies appear very close to each other on the x-axis.

It is remarkable the difference in slope between Springer's model (5.7) and the slopes that the current work yielded (28.0, 28.3 and 25.8). This indicates that the number of impacts until incubation for this coating is set with a very vertical slope and will be not easily predictable by Springer's model, although results are aligned. By looking at the past data taken to develop the model, it can be observed that the number of impacts until incubation never surpassed the value of $n_i = 10^5$. It could be possible that there is an asymptote in the curve that the model is not considering. A further refinement of the model that includes these cases would be advantageous to assess its validity with longer incubation times in polyurethane coatings.

When investigating the damage patterns in the microscope, it was noted that for lower impact frequencies, some characteristic cracks may appear (see Figure 3.25). Those cracks were correlated with valleys in the height map of the damage which seem compressive cracks. The longer droplet may increase the water-hammer pressure (and the time that this pressure holds) as well as the energy, leading to these characteristic cracks. A more prolonged lateral jetting may also explain these features, as the coating may be displaced by the jetting radially (from inside to outside the damage radius) and eventually, compressive cracks would appear. It has to be said, however, that those features were not found in every damage at 2.5 Hz. The cracks are very close to the damage and are found always around the main damaged areas. These cracks may act as nucleation points that lead to damage in the coating.

4.3 Dry intervals

The effect of the dry stops on the incubation times was studied with the ratio r (see formula 2.11). For all the combinations of the three parameters (λ, α and β), the ratios were found larger than 1, which means that incubation times increased when dry intervals were performed. Although the deviation of the results is relatively high, (up to 3 in some cases, see table 3.10), they are always contained in the range in which $r > 1$.

This increase can be explained by the viscoelastic effect of the PU coating: as the coating has more time to recover itself, improving its rain erosion performance. In this regard, the initial research hypothesis was confirmed. The different influences of the dry interval parameters can also be explained by the viscoelastic behaviour. The parameter λ represents the duration of the dry interval. The longer the dry interval, the more time the coating has to recover.

This was the trend that was found in the means effects plot (Figure 3.27). The parameter α describes the moment at which the stop was started. It was theorized that, if the stop is performed too late, the coating may already be plastically damaged and its recovery may not be complete. This is the trend that was found: for lower values of α, higher values of the ratio were found. The parameter β was not found to have an effect on the means of r. This would mean that the incubation times are not sensitive to the number of stops that were held but to the total time duration of the dry interval.

According to the Pareto chart and means effects plot (Figure 3.27), the effect of the duration of the dry interval is more significant than the moment at which it starts. This relationship may depend on the values of λ and α that were chosen in the matrix of experiments (see table 2.8). The influence of these two phenomena in the ratio is not expected to be linear: related to the interval length, at some point, it should be expected that a longer interval does not have a further effect on the incubation time, as the coating should have already had enough time to recover. In a similar way, the influence of the moment at which the dry interval starts may change when varying the parameter α: an interval with a value for α too high (this is, with a dry interval that starts late) may result in plastic damage, and it may even not recover at all. This work shows just some preliminary trends that should be further investigated. Tests with larger matrixes of experiments will likely shed light on the influence of these parameters and the overall viscoelastic behaviour of the coating.

Chapter 5

Conclusions

Incubation times of PU coated GFRP samples were studied in a PJET facility. The effect of different parameters of the test equipment was first examined: the water cushion effect, temperature and humidity. The effects of the water cushion were investigated for a fixed velocity (160 m/s) and several impact frequencies (2.7, 27.7 and 42.6 Hz). It was found that the water cushion increases the number of impacts until incubation for high frequencies (42.6 Hz) but not for medium and lower frequencies (2.5 and 27.7 Hz). Temperature and humidity were found to have an effect on the incubation times of PU coated samples: the higher the sample temperature and the higher the environmental humidity in the cabinet, the lower the incubation times. DMA analysis showed a decrease in the storage and loss modulus of the PU coating when the temperature is increased and the coating is saturated with water. These changes in the properties of the coating have been linked to the decrease in incubation times observed while testing. However, past research work suggests that this change in properties is not necessarily linked to a drop in rain erosion performance of polyurethane coatings [44] [17]. It has been hypothesised that changes in the storage and loss moduli may be provoking adhesion problems in the interphase between the coating and the substrate that lead to faster damage. These effects were considered when studying the incubation times during the project: the water cushion was removed with an air supply that the PJET incorporated. The temperature of the water and the tested sample and the relative humidity in the PJET equipment were logged; just the incubation times that were measured under determined conditions of temperature and humidity were considered in the final results (this included, for example, the consistent discard of the first measurement of the day).

The effects of impact frequency on the incubation times of PU coatings were analyzed. Curves that showed the relation between the impact velocity (v_i) and the number of impacts until incubation (n_i) were obtained for three impact frequencies ($v_i - n_i$ or Wöhler curves). It was found that the higher the impact frequency, the higher the number of impacts until incubation time. This effect was linked to the longer and more massive droplets created by the PJET for lower frequencies due to its working principle, rather than to the viscoelastic properties of the PU coating. The effect of the viscoelastic behaviour and the different relaxation times to recover from impacts may have been hindered by the change in droplet

length. When the Wöhler curves were modified to account for the cumulative impact energy of the droplets instead of the number of impacts, the values of energy were very similar for every impact frequency. The Wöhler slopes were found to be quite very similar for every impact frequency, which indicates that the effect of impact velocity on incubation times does not depend on impact frequency. The results of the number of impacts until incubation n_i were compared with Springer's models, which predict the incubation times of materials. Two Springer's models were compared: for homogeneous and coated materials. The results for low impact frequencies under-performed the expected values of Springer's model, while high impact frequencies outperformed the predicted values yielded by the model. This difference is also linked to the difference in length and energy of the droplets. It was observed that the slope of the power-law that better fitted the experimental points from the present work was much higher than the one of Springer's model: 28.0, 28.3 and 25.8 versus 5.7. The experimental points from this work are situated in an area in the Springer model that does not have any other past experimental point. This fact may be an incentive to experiment with high values of the number of impacts until incubation for Springer's model.

The effect of the performance of dry intervals in the incubation times was investigated for a fixed velocity and frequency (160 m/s and 27.7 Hz). Incubation times were found to increase by a factor of 3 to 6 when performing these intervals. The effect of different parameters which characterise the dry interval were studied. Those parameters accounted for the duration of the dry interval (λ), for the moment at which the dry interval started (α) and the number of stops that the dry interval was divided into (β). It was found a significant effect of the parameters λ and α, but not for β. This behaviour is linked to the viscoelastic material: a longer dry interval means more time for the coating to recover. If the interval starts later, plastic damage will have appeared and a full recovery could not be achieved. This finding reveals the importance of relaxation times for the coating to be recovered between impacts and the importance of establishing parameters to account for those factors in rain erosion PJET facilities.

Chapter 6

Recommendations

The present research work was aimed to investigate the change in incubation times when changing impact frequency in a PU viscoelastic coating. This observation could not be fully achieved as lower and higher frequency droplets are not directly comparable in the PJET. The droplet with a lower impact frequency has a higher length and more energy. The PJET current approach does not allow to change impact frequency without varying the impact energy per droplet, as both depend on the rotating frequency of the PJET disk (see figure 2.3). Some modifications could be implemented to the PJET to investigate the impact frequency in viscoelastic materials. One of them is the modification of the rotating disk itself. Next figure 6.1 shows a picture of the rotating disc installed in the PJET setup. Different versions of discs with a different number of holes could be manufactured. This way, the effect of the impact frequency could be observed without varying the impact frequency in the PJET parameters, but by changing the rotating disc. In the present work, it has been observed that the existence of dry intervals while testing increase the incubation time, so it seems plausible that viscoelastic effects have an effect also for lower relaxation times "between droplets".

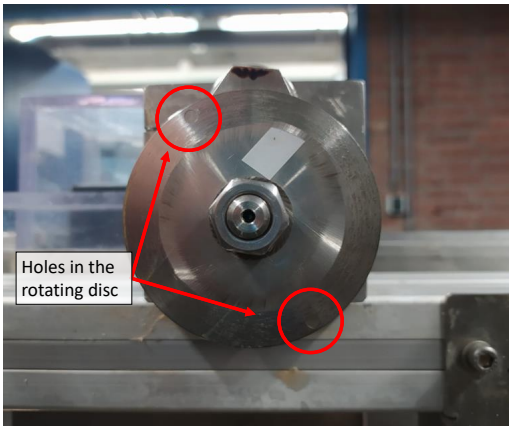

Figure 6.1: Rotating disc installed in the PJET. The two holes which cut the jet slug and create the droplets are visible.

One of the conclusions of the present work is that the performance of dry intervals while testing increase the incubation time for PU coatings. This work focused on a limited experimental matrix: just eight values for three parameters. A similar study with a larger experimental matrix is expected to provide deeper insight into the effect of the nature of dry intervals in the incubation times. Moreover, rain erosion testing with dry intervals could be developed for more viscoelastic coatings and in more testing facilities, such as the whirling arm. Further work in this direction would be very valuable for models that aim to predict the lifetime of WBT coatings. These dry intervals could be understood as "between rainfalls" periods. There are models which use stochastic and statistical information about rainfall and may be able to consider these periods during rainfalls in which the intensity is much lower (or rain stops). If the effect of the dry intervals is deeper, these models could be refined.

During the study of the impact frequency, the droplet length and droplet kinetic energy were proven to be important parameters linked to the incubation times of the coating. Researchers and/or manufacturers should document, whenever possible, the length and shape of the droplet, especially in PJET facilities, as droplets may have a cylindrical shape. This information would enable researchers to compare more effectively results among different testing facilities. Furthermore, droplet impact frequency is expected to be an important parameter for viscoelastic materials. Although this work could not link different impact frequencies with the viscoelastic behaviour of the material, the variation in the incubation times when performing dry intervals already suggest that relaxation times are beneficial for the coating. Droplet impact frequency should be documented while testing whenever possible. It has to be noted that impact frequency is one of the limitations of rain erosion testing: real-life rain droplets frequency usually ranges between 0.05 and 5 Hz depending on rainfall intensity [8], while impact frequency in test facilities is much higher (for the present project, the lowest frequency was 2.5 Hz). This difference between real-life and testing frequencies makes it important to keep track of the exact values of frequency that are tested, especially if the results are aimed to be correlated with real-life erosion. Correlation between different laboratory rain erosion testing equipments and real-life erosion evolution is very difficult [37].

It is essential to perform more tests to determine the effect of humidity and temperature on reinforced samples with PU. It has been theorized that these effects play a role as the properties of the coating change, but the exact way this happens is still not known. The effect is likely to be related to the plasticization of the coating material. More tests, such as Differential Scanning Calorimetry (DSC), could shed light on the changes in structure when PU samples get saturated or heated and will help to understand up to which point plasticization is changing the rain erosion performance of coated samples. The investigation of the reversibility of this process would also be interesting, as some shape morphing polyurethanes show high reversibility when heated after being saturated. More DMA analysis could be performed covering a wider range of temperatures to see more prominent changes in the mechanical properties of PU coatings. It would also be interesting to investigate the influence of temperature and humidity in the interphase between coating and substrate and to know how the interphase strength may change. Straights peel-up adhesion tests, such as performed by Cortés [5] may be useful in this regard.

One of the challenges that were faced was to measure the temperature of the coating while testing. Thermocouples could not be placed in the coating itself, as they were torn away by the lateral jetting, so they were placed in the back of the substrate for the present work. The temperature could increase locally at the hitting spot of the coated sample much more than

in the substrate, thus, changing the properties of the coating. Solutions need to be found to assess more accurately the temperature of the sample. One solution could be the use of thermal imaging. However, those setups should cope with the mist that comes from testing, which may be challenging.

Some modifications could be done to the PJET to improve the quality and relevance of testing results. The installation of a camera in the cabinet that may observe droplet lengths could be interesting. A camera could also provide another way to observe the moment at which damage is produced (incubation time): the cabinet full of mist and water droplets becomes a challenge when assessing incubation times. This work has highlighted the importance of controlling the humidity and temperature during testing, so those should be very controlled. The cooler could have a loop-feedback system to maintain the water at a constant temperature, rather than the cooler being on or off and wait for the water to be stabilized.

It has to be noted that the whole work has been focused on the incubation times for polyurethane coatings. The same analysis could be done to assess the mass loss and damage evolution of coatings. Other studies related to the roughness of the coating while tested are promising, as roughness has been proven a good parameter to assess rain erosion [17].

Annex I

Theoretical determination of the droplet length (PJET)

An estimation of the droplet length depending on the impact frequency was carried out. This annexe will address the assumptions that were made and the steps to get to the values of the theoretical length.

The impact frequency depends on the frequency of the rotating disk. This disk has holes that allow the jet to go through it and create the droplets. These two frequencies are different. As the rotating disk has two holes, its rotating frequency is two times the impact frequency. The rotating frequency of the disc is given by the DUCOM PJET manual. Droplet impact frequencies were calibrated before carrying out the experiments.

The geometry of the disk is known. The diameter of the circle that contains both holes is 35 mm. The holes have a diameter of 1.5 mm. The water jet expelled by the nozzle was estimated to be 1.5 mm in diameter. This is the value of the diameter nozzle according to the DUCOM manual.

The nozzle ejects the water jet that is cut by the rotating disk. When the jet meets the holes, water goes through the hole and the droplet is created. The "effective time" is the time at which the water jet goes through the hole and creates the droplet. To estimate droplet length, it was considered that as soon as the water jet meets the hole, the water droplet starts to be created. When the water jet stops meeting the hole, the droplet stops being formed. This is what was called the effective time t_{ef}. This is the same assumption used by other authors, as Jonnson [10].

Graphically, the problem can be simplified because the radius diameter is small compared to the radius of the rotating disk. The ratio between those two values is higher than 20. This geometry allows being simplified using the small-angle approximation. This approximation has an error of <1% for angles of 14º, while this angle is around 3º (look for reference). The parameter d_h refers to the diameter of the hole in the disk, while r_{disk} is the radius from the centre of the disk up to the hole.

$$sin(\frac{\alpha}{2}) = \frac{d_h/2}{r_{disk}}$$

$$\alpha \sim \frac{d_h}{r_{disk}}$$

Looking at the diagram, the effective time can be analytically obtained, being f_{disk} the frequency of the rotating disk (not the impact frequency).

$$t_{ef} = \frac{2d_h}{r} \cdot \frac{1}{2\pi f_{disk}} \tag{I.1}$$

The values of impact frequencies are known from the DUCOM manual and calibration: 2.7 Hz and 47.7 Hz. However, those are the impact frequencies, not the rotating frequencies of the disk. The rotating disk has two holes that form droplets, so the rotating frequency of the disk is half the impact frequency.

$$f_{disk} = \frac{f_i}{2} \tag{I.2}$$

$$t_{ef} = \frac{2d_h}{r_{disk}} \cdot \frac{1}{\pi f_i} \tag{I.3}$$

The length of the droplet is the result of multiplying the time that the nozzle is ejecting water through the hole (the effective time t_{ef}) with the impact velocity (v_i).

$$l_{drop} = t_{ef} \cdot v_i \tag{I.4}$$

$$l_{drop} = \frac{2d_h}{r_{disk}} \cdot \frac{1}{\pi f_i} \cdot v_i \tag{I.5}$$

This is the final equation that was used to obtain the theoretical droplet lengths that appear in table 3.8. I may add a plot about this.

References

[1] London summit 2017, bloomberg. new energy finance. it does not appear yet. Accessed: 2020-09-14.

[2] Hamish Macdonald, David Infield, David H Nash, and Margaret M Stack. Mapping hail meteorological observations for prediction of erosion in wind turbines. *Wind Energy*, 19(4):777–784, 2016.

[3] Mark Hugh Keegan, David Nash, and Margaret Stack. *Wind Turbine Blade Leading Edge Erosion: An investigation of rain droplet and hailstone impact induced damage mechanisms*. PhD thesis, University of Strathclyde, 2014.

[4] Omid Gohardani. Impact of erosion testing aspects on current and future flight conditions. *Progress in Aerospace Sciences*, 47(4):280–303, 2011.

[5] Enrique Cortés, Fernando Sánchez, Anthony O'Carroll, Borja Madramany, Mark Hardiman, and Trevor M Young. On the material characterisation of wind turbine blade coatings: the effect of interphase coating–laminate adhesion on rain erosion performance. *Materials*, 10(10):1146, 2017.

[6] Uurgegevens van het weer in Nederland knmi. https://www.knmi.nl/nederland-nu/klimatologie/uurgegevens. Accessed: 2-08-2021.

[7] Mohamed Elhadi Ibrahim and Mamoun Medraj. Water droplet erosion of wind turbine blades: Mechanics, testing, modeling and future perspectives. *Materials*, 13(1):157, 2020.

[8] AF Conn and SL Rudy. Effects of fatigue and dynamic recovery on rain erosion. In *Erosion, wear, and interfaces with corrosion*. ASTM International, 1974.

[9] EF Tobin, TM Young, D Raps, and O Rohr. Comparison of liquid impingement results from whirling arm and water-jet rain erosion test facilities. *Wear*, 271(9-10):2625–2631, 2011.

[10] Robert Jonsson. Characterisation and validation of a pulsating jet erosion test, 2007.

[11] Wind energy international, 2019. https://library.wwindea.org/. Accessed: 2020-09-14.

[12] Bureau of ocean energy management boem. renewable energy on the outer continental shelf. https://www.boem.gov/renewable-energy/renewable-energy-program-overview. Accessed: 2020-09-14.

[13] Agrim Sareen, Chinmay A Sapre, and Michael S Selig. Effects of leading edge erosion on wind turbine blade performance. *Wind Energy*, 17(10):1531–1542, 2014.

[14] Woobeom Han, Jonghwa Kim, and Bumsuk Kim. Effects of contamination and erosion at the leading edge of blade tip airfoils on the annual energy production of wind turbines. *Renewable energy*, 115:817–823, 2018.

[15] Leon Mishnaevsky Jr. Toolbox for optimizing anti-erosion protective coatings of wind turbine blades: Overview of mechanisms and technical solutions. *Wind Energy*, 22(11):1636–1653, 2019.

[16] Stanley Smith Cook. Erosion by water-hammer. *Proceedings of the Royal Society of London. Series A, Containing Papers of a Mathematical and Physical Character*, 119(783):481–488, 1928.

[17] Anthony O'Carroll. Correlation of mechanical properties to rain erosion resistance of polymeric materials. 2018.

[18] Denis Bartolo, Christophe Josserand, and Daniel Bonn. Singular jets and bubbles in drop impact. *Physical review letters*, 96(12):124501, 2006.

[19] FJ Heymann. High-speed impact between a liquid drop and a solid surface. *Journal of Applied Physics*, 40(13):5113–5122, 1969.

[20] Akbar Hojjati Najafabadi, Reza Shoja Razavi, Reza Mozaffarinia, and Hamed Rahimi. A new approach of improving rain erosion resistance of nanocomposite sol-gel coatings by optimization process factors. *Metallurgical and Materials Transactions A*, 45(5):2522–2531, 2014.

[21] K Fujisawa, T Yamagata, and N Fujisawa. Damping effect on impact pressure from liquid droplet impingement on wet wall. *Annals of Nuclear Energy*, 121:260–268, 2018.

[22] HH Shi, JE Field, and CSJ Pickles. High speed liquid impact onto wetted solid surfaces. 1994.

[23] Shizhong Zhang, Kim Dam-Johansen, Sten Nørkjær, Pablo L Bernad Jr, and Søren Kiil. Erosion of wind turbine blade coatings–design and analysis of jet-based laboratory equipment for performance evaluation. *Progress in Organic Coatings*, 78:103–115, 2015.

[24] Robbie Herring, Kirsten Dyer, Ffion Martin, and Carwyn Ward. The increasing importance of leading edge erosion and a review of existing protection solutions. *Renewable and Sustainable Energy Reviews*, 115:109382, 2019.

[25] Amrit Shankar Verma, Zhiyu Jiang, Zhengru Ren, Marco Caboni, Hans Verhoef, Harald van der Mijle-Meijer, Saullo GP Castro, and Julie JE Teuwen. A probabilistic long-term framework for site-specific erosion analysis of wind turbine blades: A case study of 31 dutch sites. *Wind Energy*, 2021.

[26] JO Haerter, P Berg, and S Hagemann. Heavy rain intensity distributions on varying time scales and at different temperatures. *Journal of Geophysical Research: Atmospheres*, 115(D17), 2010.

[27] Olive G Engel. Waterdrop collisions with solid surfaces. *Journal of research of the national bureau of standards*, 54(5):281–298, 1955.

[28] C Hasager, F Vejen, JI Bech, WR Skrzypiński, A-M Tilg, and M Nielsen. Assessment of the rain and wind climate with focus on wind turbine blade leading edge erosion rate and expected lifetime in danish seas. *Renewable Energy*, 149:91–102, 2020.

[29] HM Slot, ERM Gelinck, C Rentrop, and Emile Van Der Heide. Leading edge erosion of coated wind turbine blades: Review of coating life models. *Renewable Energy*, 80:837–848, 2015.

[30] Drew Eisenberg, Steffen Laustsen, and Jason Stege. Wind turbine blade coating leading edge rain erosion model: Development and validation. *Wind Energy*, 21(10):942–951, 2018.

[31] HM Slot, RM IJzerman, M Le Feber, K Nord-Varhaug, and Emile van der Heide. Rain erosion resistance of injection moulded and compression moulded polybutylene terephthalate pbt. *Wear*, 414:234–242, 2018.

[32] George S Springer. Erosion by liquid impact. 1976.

[33] MA Miner et al. Cumulative fatigue damage. *Journal of applied mechanics*, 12(3):A159–A164, 1945.

[34] George S Springer and CB Baxil. A model for rain erosion of homogeneous materials. In *Erosion, Wear, and Interfaces with Corrosion*. ASTM International, 1974.

[35] George S Springer, Cheng-I Yang, and Poul S Larsen. Analysis of rain erosion of coated materials. *Journal of Composite Materials*, 8(3):229–252, 1974.

[36] Benjamain Luiset, Frederic Sanchette, Alain Billard, and D Schuster. Mechanisms of stainless steels erosion by water droplets. *Wear*, 303(1-2):459–464, 2013.

[37] Luis Bartolomé and Julie Teuwen. Prospective challenges in the experimentation of the rain erosion on the leading edge of wind turbine blades. *Wind Energy*, 22(1):140–151, 2019.

[38] Amrit Shankar Verma, Saullo GP Castro, Zhiyu Jiang, and Julie JE Teuwen. Numerical investigation of rain droplet impact on offshore wind turbine blades under different rainfall conditions: A parametric study. *Composite Structures*, page 112096, 2020.

[39] Blade protection coating w4600 - technical data sheet and application guide. 2014. https://multimedia.3m.com/mws/media/9788680/3m-wind-blade-coating-w4600-app-guide-and-technical. Accessed: 17-04-2021.

[40] Class instrumentation ltd. class instrumentation ltd ultrasonic sound velocity table. http://www.classltd.com/sound_velocity_table.html. Accessed: 17-04-2021.

[41] A Déom, R Gouyon, and C Berne. Rain erosion resistance characterizations: Link between on-ground experiments and in-flight specifications. *Wear*, 258(1-4):545–551, 2005.

[42] ASTM Standard. D3574-11 "standard test methods for flexible cellular materials-slab, bonded, and molded urethane foams". *Internet). ASTM Int*, 2014.

[43] I Ouachan, M Kuball, D Liu, K Dyer, C Ward, and I Hamerton. Und erstanding of leading-edge protection performance using nano-silicates for modification. In *Journal of Physics: Conference Series*, volume 1222, page 012016. IOP Publishing, 2019.

[44] G Arena, K Friedrich, D Acierno, E Padenko, P Russo, G Filippone, and J Wagner. Solid particle erosion and viscoelastic properties of thermoplastic polyurethanes. *Express Polymer Letters*, 9(3), 2015.

[45] Debra Dunson. Characterization of polymers using dynamic mechanical analysis (dma). *EAG Appl Note*, 2017.

[46] Testing of rotor blade erosion protection systems, 2018. https://rules.dnvgl.com/docs/pdf/DNVGL/RP/2018-02/DNVGL-RP-0171.pdf. Accessed: 2021-05-08.

[47] George S Springer and Cheng I Yang. Model for the rain erosion of fiber reinforced composites. *AIAA journal*, 13(7):877–883, 1975.

[48] Goodness of fit for Individual Distribution Identification minitab 19 support. https://support.minitab.com/en-us/minitab/19/help-and-how-to/quality-and-process-improvement/quality-tools/how-to/individual-distribution-identification/interpret-the-results/all-statistics-and-graphs/goodness-of-fit/. Accessed: 19-06-2021.

[49] Interpret all statistics for a probability plot with lognormal fit, howpublished = https://support.minitab.com/en-us/minitab-express/1/help-and-how-to/graphs/probability-plot/interpret-the-results/all-statistics/probability-plot-with-lognormal-fit/, note = Accessed: 11-08-2021.

[50] Interpret the key results for Analyze Factorial Design minitab 19 support. https://support.minitab.com/en-us/minitab/18/help-and-how-to/modeling-statistics/doe/how-to/factorial/analyze-factorial-design/interpret-the-results/key-results/. Accessed: 20-06-2021.

[51] Effects plots for Analyze Factorial Design, howpublished = https://support.minitab.com/en-us/minitab/18/help-and-how-to/modeling-statistics/doe/how-to/factorial/analyze-factorial-design/methods-and-formulas/effects-plots/#lenth-s-pseudo-standard-error-pse, note = Accessed: 11-08-2021.

[52]

[53] How (and when) to use anova in excel: The ultimate guide. https://www.goskills.com/Lean-Six-Sigma/Resources/Use-anova-in-Excel, note = Accessed: 19-06-2021.

[54] ASTM Standard. Astm g73 - 10 "standard test method for liquid impingement erosion using rotating apparatus". *Internet). ASTM Int*, 2017.

[55] MS Mahdipoor, HS Kirols, D Kevorkov, P Jedrzejowski, and M Medraj. Influence of impact speed on water droplet erosion of tial compared with ti6al4v. *Scientific reports*, 5:14182, 2015.

[56] LI Seleznev, VA Ryzhenkov, and AF Mednikov. Phenomenology of erosion wear of constructional steels and alloys by liquid particles. *Thermal engineering*, 57(9):741–745, 2010.

[57] JH Brunton. A discussion on deformation of solids by the impact of liquids, and its relation to rain damage in aircraft and missiles, to blade erosion in steam turbines, and to cavitation erosion-high speed liquid impact. *Philosophical Transactions of the Royal Society of London. Series A, Mathematical and Physical Sciences*, 260(1110):79–85, 1966.

[58] Ruizi Zhang, Bin Zhang, Qian Lv, Jingyin Li, and Penghua Guo. Effects of droplet shape on impact force of low-speed droplets colliding with solid surface. *Experiments in Fluids*, 60(4):1–13, 2019.

[59] Shizhong Zhang, S Kiil, K Dam-Johansen, and PL Bernad Jr. Accelerated rain erosion of wind turbine blade coatings. *Danmarks Tekniske Universitet (DTU)*, 2014.

[60] Ya-Jen Yu, Keith Hearon, Thomas S Wilson, and Duncan J Maitland. The effect of moisture absorption on the physical properties of polyurethane shape memory polymer foams. *Smart Materials and Structures*, 20(8):085010, 2011.

[61] A Boubakri, K Elleuch, N Guermazi, and HF Ayedi. Investigations on hygrothermal aging of thermoplastic polyurethane material. *Materials & Design*, 30(10):3958–3965, 2009.

[62] A Boubakri, Nader Haddar, K Elleuch, and Yves Bienvenu. Impact of aging conditions on mechanical properties of thermoplastic polyurethane. *Materials & Design*, 31(9):4194–4201, 2010.

[63] RN Jana and H Bhunia. Accelerated hygrothermal and uv aging of thermoplastic polyurethanes. *High Performance Polymers*, 22(1):3–15, 2010.

[64] Bin Yang, Wei Min Huang, Chuan Li, and Jun Hoe Chor. Effects of moisture on the glass transition temperature of polyurethane shape memory polymer filled with nano-carbon powder. *European Polymer Journal*, 41(5):1123–1128, 2005.

[65] Shuji Hattori and Gang Lin. Effect of droplet diameter on liquid impingement erosion. In *AIP Conference Proceedings*, volume 1428, pages 191–198. American Institute of Physics, 2012.